© 2020. Published by The Company of Biologists Ltd | Development (2020) 147, dev186841. doi:10.1242/dev.186841

RESEARCH ARTICLE

PBX1 acts as terminal selector for olfactory bulb dopaminergic neurons

Laura Remesal[1,*,‡], Isabel Roger-Baynat[1,‡], Laura Chirivella[1], Miren Maicas[1], Rebeca Brocal-Ruiz[1], Ana Pérez-Villalba[2], Carme Cucarella[3], Marta Casado[3] and Nuria Flames[1,§]

ABSTRACT

Neuronal specification is a protracted process that begins with the commitment of progenitor cells and culminates with the generation of mature neurons. Many transcription factors are continuously expressed during this process but it is presently unclear how these factors modify their targets as cells transition through different stages of specification. In olfactory bulb adult neurogenesis, the transcription factor PBX1 controls neurogenesis in progenitor cells and the survival of migrating neuroblasts. Here, we show that, at later differentiation stages, PBX1 also acts as a terminal selector for the dopaminergic neuron fate. PBX1 is also required for the morphological maturation of dopaminergic neurons and to repress alternative interneuron fates, findings that expand the known repertoire of terminal-selector actions. Finally, we reveal that the temporal diversification of PBX1 functions in neuronal specification is achieved, at least in part, through the dynamic regulation of alternative splicing. In *Caenorhabditis elegans*, PBX/CEH-20 also acts as a dopaminergic neuron terminal selector, which suggests an ancient role for PBX factors in the regulation of terminal differentiation of dopaminergic neurons.

KEY WORDS: Neuron differentiation, Alternative splicing, Terminal selector, Dopaminergic neuron, Olfactory bulb, Adult neurogenesis

INTRODUCTION

Mature neurons are specialized cells that express unique transcriptomes for specific functions. The acquisition of neuron type-specific transcriptomes is a protracted process beginning with the commitment of progenitors, followed by the migration of neuroblasts and culminating in the terminal differentiation of the neuron (Rubenstein and Rakic, 2013). Transcription factors (TFs) are the main orchestrators of neuron-type specification and different TFs fulfill specific functions at each step in this process.

Although most attention has been given to TFs with temporally or spatially restricted expression, many TFs are continuously expressed in the nervous system throughout the various stages of differentiation, from progenitors to mature neurons (Delile et al., 2019; Mayer et al., 2018; Mi et al., 2018; Nowakowski et al., 2017). In only a few cases have the specific roles of these TFs in progenitors and postmitotic neurons been determined, such as the diverse functions of *Nkx2.1* in the subpallium (Magno et al., 2011; Nóbrega-Pereira et al., 2008; Sussel et al., 1999), or the specific roles of *Fezf2*, *Brn1/2* and *Cux1/2* at particular differentiation stages in the pallium (Cubelos et al., 2008; Guo et al., 2013; Iulianella et al., 2008; Lodato et al., 2014; McEvilly et al., 2002; Sugitani et al., 2002). However, only early roles have generally been studied for these TFs, whereas later functions in postmitotic neurons have not yet been analyzed. In addition, how a TF that is continuously expressed from progenitors to mature neurons temporally modifies its activity throughout differentiation is an important unresolved issue.

In contrast to our limited understanding in mammals, neuronal terminal differentiation programs have been extensively characterized in *Caenorhabditis elegans*. In this simple model organism, specific TFs, termed terminal selectors, directly regulate the coordinated expression of the genes that allow for neuron-type-specific functions, such as neurotransmitter biosynthesis enzymes, ion channels and neurotransmitter receptors (Hobert, 2011). An increasing number of examples show that the terminal selector model also applies to mammals (Deneris and Hobert, 2014; Hobert and Kratsios, 2019). However, the extent to which specific regulatory programs are conserved throughout evolution has yet to be determined.

In *C. elegans*, CEH-20, a PBX TF, acts as a terminal selector of dopaminergic (DA) neurons (Doitsidou et al., 2013). CEH-20 works in a TF collective, together with the E26 transformation-specific TF AST-1 and the DLX homeodomain TF CEH-43 (Doitsidou et al., 2013). Remarkably, mouse orthologs for AST-1 and CEH-43, ETV1 (also called ER81) and DLX2, respectively, are required in the differentiation of olfactory bulb (OB) DA neurons, which constitute the most ancestral DA population of the mammalian brain (Brill et al., 2008; Cave et al., 2010; Flames and Hobert, 2009; Qiu et al., 1995). These data suggest that the DA neuron terminal differentiation program could be conserved from worms to mammals. However, the role of PBX TFs as OB DA terminal selectors has not been previously studied.

OB DA neurons are GABAergic interneurons located in the periglomerular layer (PGL) (Kosaka and Kosaka, 2016). These neurons are generated throughout the life of the animal from adult neural stem cell progenitors located in the subependymal zone (SEZ) (Bonzano et al., 2016). PBX1 is expressed in SEZ progenitors and early deletion of *Pbx1* and *Pbx2* leads to adult neurogenesis defects and cell death of migrating neuroblasts (Grebbin et al., 2016). These phenotypes allowed the assignment of specific early functions to PBX TFs in adult neurogenesis but precluded the study of their role in DA neuron terminal differentiation.

[1]Developmental Neurobiology Unit, Instituto de Biomedicina de Valencia, IBV-CSIC, 46010 Valencia, Spain. [2]Centro de Investigación Biomédica en Red sobre Enfermedades Neurodegenerativas (CIBERNED), Estructura de Recerca Interdisciplinar en Biotecnologia i Biomedicina (ERI BIOTECMED), and Departamento de Biología Celular, Biología Funcional y Antropología Física, Universidad de Valencia, 46100 Burjassot, Spain. [3]Centro de Investigación Biomédica en Red de Enfermedades Hepáticas y Digestivas (CIBERehd), Instituto de Salud Carlos III (ISCIII), Metabolic Experimental Pathology Unit, Instituto de Biomedicina de Valencia, IBV-CSIC, 46010 Valencia, Spain.
*Present address: School of Medicine, University of California San Francisco, United States.

‡These authors contributed equally to this work

§Author for correspondence (nflames@ibv.csic.es)

A.P-V., 0000-0002-5330-2374; N.F., 0000-0003-0961-0609

Received 27 November 2019; Accepted 24 February 2020

Development (2020) 147, dev186841. doi:10.1242/dev.186841

Here, we specifically remove *Pbx1* from terminally differentiating DA neurons and show that PBX1 is required for the correct expression of many OB DA effector genes, supporting its role as a DA terminal selector. In addition, we find PBX1 is also necessary for inducing OB DA neuron morphological maturation and for repressing alternative interneuron fates, expanding the functional repertoire of terminal-selector actions. Notably, we find that temporal PBX1 diversification of labor throughout adult neurogenesis is achieved, at least in part, by dynamic regulation of alternative splicing.

RESULTS

PBX1 but not PBX2 is required for olfactory bulb dopaminergic neuron terminal differentiation

Three TFs act as terminal selectors for *C. elegans* DA neuron differentiation: the ETS TF AST-1, the homeodomain TF CEH-43 and the PBX TF CEH-20 (Doitsidou et al., 2013). In mice, ETV1 (an ortholog of AST-1) and DLX2 (an ortholog of CEH-43) are required for DA specification in the OB (Brill et al., 2008; Cave et al., 2010; Flames and Hobert, 2009; Qiu et al., 1995), raising the possibility that the DA terminal differentiation program might be conserved from worms to mammals. Hence, we addressed whether PBX TFs are also required for correct DA terminal differentiation in the OB.

Expression of terminal selectors often continues throughout the life of the animal to maintain cell fate (Deneris and Hobert, 2014). Thus, we first analyzed the expression of the four PBX TF members in adult OB DA neurons. PBX4 is not expressed in the brain and PBX3 is expressed in OB but not in DA neurons (Grebbin et al., 2016; Fig. S1). PBX1 is expressed in OB DA neurons (Grebbin et al., 2016; Fig. S1) and similarly, we found that PBX2 expression colocalizes with tyrosine hydroxylase (TH), a marker for DA neurons in the OB (Fig. S1). Therefore, PBX1 and PBX2 are good candidates for being involved in OB DA neuron terminal differentiation; thus, we next analyzed mouse mutant models for these TFs.

To avoid known neurogenesis defects upon *Pbx1* removal from adult neuronal progenitors (Grebbin et al., 2016), we used a conditional *Pbx1* allele ($Pbx1^{Fl/Fl}$) combined with the tyrosine hydroxylase (Th) CRE recombinase knock-in line ($Pbx1^{Fl/Fl}$/*Th:CRE*, referred to as $Pbx1^{Th}$ for simplicity). Transcription of *Th* begins during the final stages of neuroblast migration, once immature DA neurons have reached the external granular layer (Saino-Saito et al., 2004; Fig. S2). Thus, $Pbx1^{Th}$ mutant animals preserve PBX1 expression in progenitors and migrating neuroblasts but not in terminally differentiating DA neurons (Figs S3 and S4). We confirmed that $Pbx1^{Th}$ animals show normal proliferation and migration by quantifying the number of proliferating cells (Ki67 positive) in the SEZ and the number of migrating neuroblasts [doublecortin (DCX) positive] in the rostral migratory stream (RMS) (Fig. S3). In contrast to PBX1, PBX2 is not expressed in SEZ progenitors or in migrating neuroblasts (Fig. S1) and therefore, we used *Pbx2* conventional knockout mice ($Pbx2^{-/-}$) to assess its role in OB DA terminal differentiation.

TH immunohistochemical analysis shows similar numbers of DA cells in the OB of $Pbx2^{-/-}$ mutants and control animals; however, there is a dramatic decrease of TH expression in adult $Pbx1^{Th}$ mice, suggesting a role for this TF in DA terminal differentiation (Fig. 1A-C,E; Table S1). In other cellular contexts, *Pbx2* acts redundantly with *Pbx1* (Capellini et al., 2008; Ferretti et al., 2011; Grebbin et al., 2016; Koss et al., 2012). Thus, to unravel possible compensatory effects, we analyzed the OB DA population of $Pbx1^{Th}$, $Pbx2^{-/-}$ double-mutant mice. We found that the $Pbx1^{Th}$ phenotype is not significantly increased in the $Pbx1^{Th}$, $Pbx2^{-/-}$ double mutant (Fig. 1D,E; Table S1), indicating that *Pbx1* plays a major role in OB DA neuron terminal differentiation that cannot be offset by the presence of *Pbx2*. Therefore, we specifically focused the rest of our analyses on $Pbx1^{Th}$ single mutant characterization.

PBX1 function is dispensable for survival of olfactory bulb dopaminergic neurons

The observed loss of TH expression in $Pbx1^{Th}$ mutant mice might reflect either DA terminal differentiation problems or survival defects. Early *Pbx1* removal from migrating neuroblasts leads to cell death (Grebbin et al., 2016). Thus, we next attempted to directly assess DA neuron survival in $Pbx1^{Th}$ animals. To this purpose, we performed DA lineage-tracing analysis introducing the fluorescent reporter R26R CAG-boosted EGFP LoxP allele (*RCE:loxP*) into $Pbx1^{Th}$ and control mice (Fig. 1F). Quantification of GFP-expressing cells showed no difference between $Pbx1^{Th}$ and control animals (Fig. 1G-I; Table S1). Moreover, immunostaining against the apoptotic marker cleaved caspase 3 showed no differences between control and mutant animals (Fig. S4). These results demonstrate that, in contrast to the earlier role of PBX1 in the survival of adult-generated migrating neuroblasts (Grebbin et al., 2016), PBX1 is not required for OB DA neuron survival at later stages of differentiation. The divergent phenotypes generated upon *Pbx1* removal at distinct differentiation steps uncover stage-specific functions for PBX1.

PBX1 controls embryonic and adult-generated olfactory bulb dopaminergic-neuron differentiation

OB DA neurons are classified into two subpopulations with different morphologies and electrophysiological properties (Galliano et al., 2018; Kiyokage et al., 2010; Kohwi et al., 2007; Kosaka and Kosaka, 2016; Vergaño-Vera et al., 2006). Generation of both DA neuron subtypes is temporally segregated: embryonically generated DA neurons are larger in size, have more complex morphologies and contain axon initial segment, whereas postnatal adult neurogenesis generates smaller DA neurons that lack an axon initial segment (Galliano et al., 2018).

To investigate the role of PBX1 in embryonically generated DA neurons, newborn $Pbx1^{Th}$ animals were analyzed. At postnatal day 0 (P0), $Pbx1^{Th}$ mutant mice already showed a significant decrease in the number of TH-positive cells in the OB compared with control animals (Fig. 1J-L; Table S1), indicating that PBX1 is required for terminal differentiation of embryonically generated DA neurons.

Embryonic DA-specification defects could explain per se adult $Pbx1^{Th}$ mutant decreases in the number of TH-positive cells (Fig. 1E). Thus, to unequivocally assess whether PBX1 has a role in the specification of adult-generated DA neurons, 2-month-old control and $Pbx1^{Th}$ animals were injected with bromodeoxyuridine (BrdU), a thymidine analog, to label adult proliferating progenitors. Animals were sacrificed 42 days after injections to allow for migration and differentiation of the adult-generated cohort of cells (Fig. 1M). The total number of BrdU-positive cells was unaffected in $Pbx1^{Th}$ animals (Fig. 1N; Table S1), although there was a significant decrease in the number of double-labeled TH- and BrdU-positive cells compared with control animals (Fig. 1O; Table S1). This indicates a role for PBX1 in the terminal specification of adult-generated DA neurons and confirms cell survival is not affected in $Pbx1^{Th}$ animals. As expected, the deletion of *Pbx1* exclusively from the DA lineage ($Pbx1^{Th}$) did not affect the other two types of adult-generated periglomerular interneurons labeled with calretinin (CR) and calbindin (CB) (Fig. 1P,Q; Table S1). Nevertheless, we found that PBX1 is expressed in 16% of CR and 42% of CB interneurons (Fig. S4). PBX1 expression in non-DA lineages is unaffected in

Development (2020) 147, dev186841. doi:10.1242/dev.186841

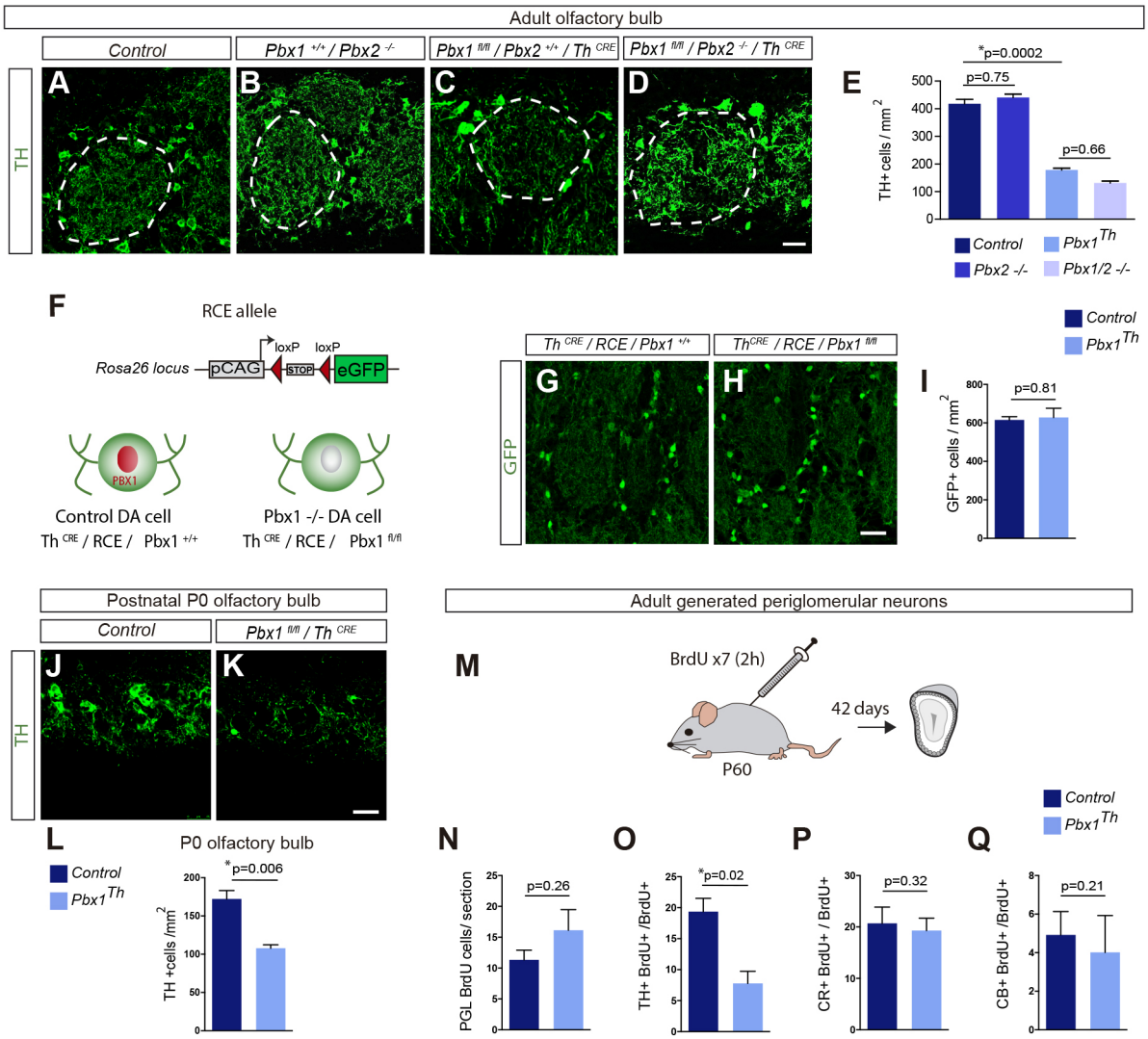

Fig. 1. PBX1 is required for olfactory bulb dopaminergic neuron terminal differentiation but not cell survival. (A-D) Tyrosine hydroxylase (TH) expression in control (A), *Pbx2* mutants (B), *Pbx1*Th mutants (C), and double *Pbx1*Th and *Pbx2* mutants (D). (E) Quantification of the different genotypes. *n*=3 animals for each condition, Tukey's multiple comparison test. (F) Diagram of the RCE allele. Cells expressing CRE recombinase become permanently labeled with GFP. (G,H) GFP-positive cells in control animals (G) and *Pbx1*Th mutant animals (H). (I) Quantification of GFP-positive cells in controls and *Pbx1*Th mutants. *n*=3 animals for each condition, two-tailed unpaired Student's *t*-test. (J,K) Tyrosine hydroxylase expression at postnatal day 0 in controls (J) and *Pbx1*Th mutants (K). (L) Quantification of TH-positive cells in controls and *Pbx1*Th mutants in P0 OB. *n*=3 animals each condition, two-tailed unpaired Student's *t*-test. (M) Experimental design for labeling adult-generated OB neurons. (N) Quantification of total number of BrdU cells/section. *n*=3 animals for each condition, two-tailed unpaired Student's *t*-test. (O-Q) Percentage of BrdU cells expressing TH, CR and CB in controls and *Pbx1*Th mutants. *n*=3 animals, two-tailed unpaired Student's *t*-test. Scale bars: 25 µm. See Table S1 for primary data for quantification, Fig. S1 for PBX2 expression analysis in SEZ, RMS and OB, and Fig. S2-S4 for *Th*^{CRE} expression analysis and *Pbx1* deletion analysis in *Pbx1*Th mutants.

Pbx1Th animals, thus the role of PBX1 on CR and CB differentiation remains to be explored. Altogether, our results demonstrate that PBX1 is necessary for terminal differentiation of both embryo- and adult-generated OB DA neurons.

PBX1 acts downstream of or in parallel to other transcription factors required for dopaminergic neuron specification

Several TFs are known to be required for correct OB DA neuron specification, including previously mentioned orthologs of *C. elegans* DA terminal selectors DLX2 (Brill et al., 2008; Qiu et al., 1995) and ETV1 (Cave et al., 2010; Flames and Hobert, 2009), and also PAX6 paired homeodomain (Brill et al., 2008; Hack et al., 2005; Kohwi et al., 2007), NR2F1 (also known as COUP-TF1) nuclear hormone receptor (Bovetti et al., 2013; Zhou et al., 2015) and MEIS2 TALE homeodomain (Agoston et al., 2014). In common with PBX1, all of these TFs are expressed throughout the DA differentiation process from progenitors and migrating neuroblasts to postmitotic DA neurons. As we saw in *Pbx1*Th mutant mice, loss-of-function experiments for these TFs lead to lower numbers of TH-expressing cells (Agoston et al., 2014; Bovetti et al., 2013; Brill et al., 2008; Flames and Hobert, 2009). Considering these phenotypic similarities, we next analyzed whether PBX1 acts upstream of any of these TFs.

Double-immunostaining analysis of TF expression in the DA lineage showed that COUP-TF1, ETV1 and PAX6 expression remained unaffected in *Pbx1*Th animals, suggesting that PBX1 acts downstream of or in parallel to these TFs (Fig. 2A-I; Table S1). *Pbx1*Th mutant mice showed a small increase in the number of DA lineage cells co-expressing DLX TFs (Fig. 2J-L; Table S1), demonstrating PBX1 is not required for DLX expression. The potential biological relevance of the increase of DLX-expressing

Development (2020) 147, dev186841. doi:10.1242/dev.186841

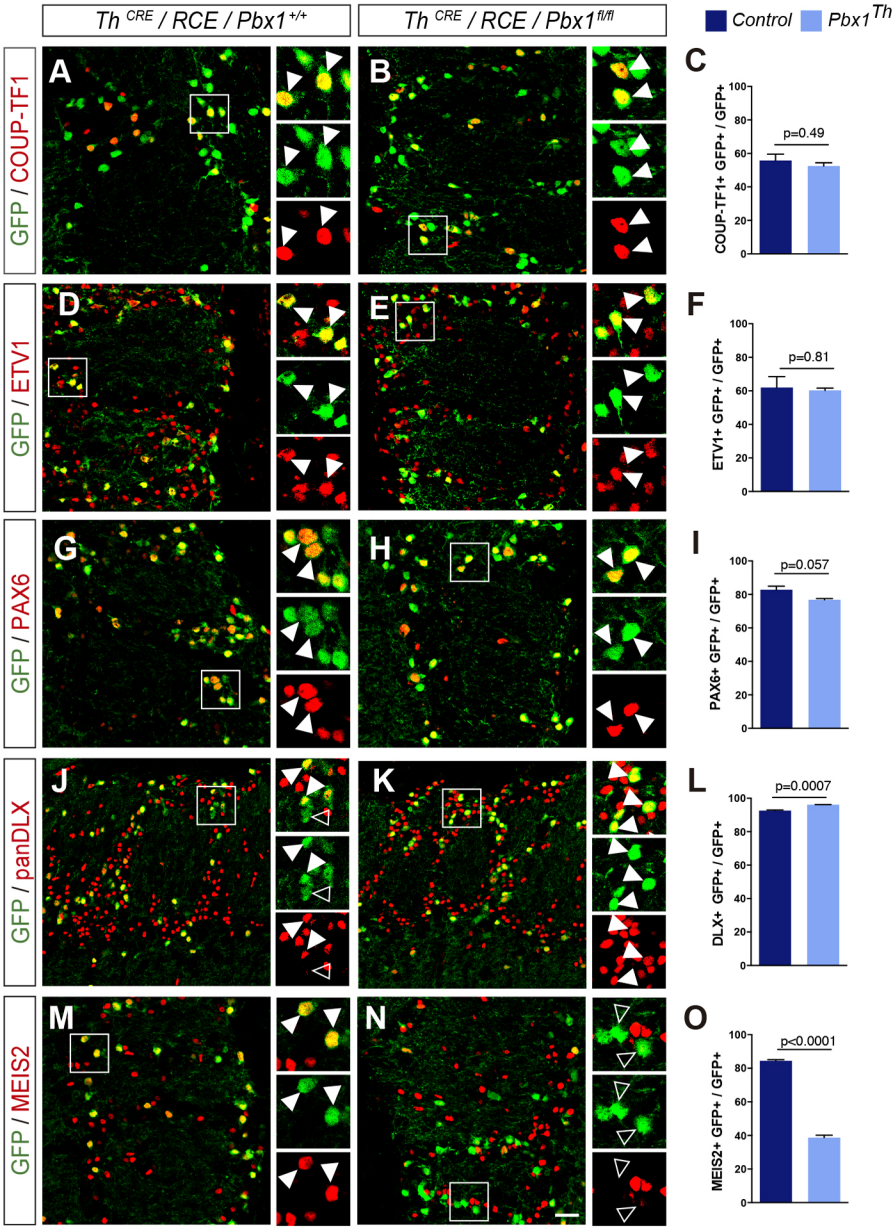

Fig. 2. PBX1 acts downstream or in parallel to other TFs required for DA specification. (A,B) COUP-TF1 expression in DA lineage cells of controls and *Pbx1*Th mutants. (C) Quantification of double COUP-TF1/GFP-positive cells. *n*=3 animals for each condition, two-tailed unpaired Student's *t*-test. (D,E) ETV1 expression in DA lineage cells of controls and *Pbx1*Th mutants. (F) Quantification of double ETV1-/GFP-positive cells. *n*=3 animals for each condition, two-tailed unpaired Student's *t*-test. (G,H) PAX6 expression in DA lineage cells of controls and *Pbx1*Th mutants. (I) Quantification of double PAX6-/GFP-positive cells. *n*=3 animals for each condition, two-tailed unpaired Student's *t*-test. (J,K) panDLX expression in DA lineage cells of controls and *Pbx1*Th mutants. (L) Quantification of double DLX-/GFP-positive cells. *n*=3 animals each condition, two-tailed unpaired Student's *t*-test. (M,N) MEIS2 expression in DA lineage cells of controls and *Pbx1*Th mutants. (O) Quantification of double MEIS2-/GFP-positive cells. *n*=3 animals each condition, two-tailed unpaired Student's *t*-test. Scale bar: 25 µm. See Table S1 for primary data for quantification and Fig. S5 for *Meis2* mRNA expression analysis by qPCR. *Meis2* transcription is unaffected in *Pbx1*Th mutants. White arrowheads indicate colocalization; black arrowheads indicate lack of colocalization.

cells is so far unclear. Finally, immunohistochemical analysis revealed a decrease in the number of MEIS2-positive cells in the DA lineage of *Pbx1*Th animals, indicating that PBX1 is required for correct MEIS2 protein expression (Fig. 2M-O; Table S1). When co-expressed in the same cell, PBX and MEIS TFs function as protein complexes (Longobardi et al., 2014). PBX1 has not been reported to transcriptionally activate *Meis2*; however, in other cellular contexts, *Pbx1* loss leads to MEIS2 protein instability and degradation (Dardaei et al., 2014; Garcia-Cuellar et al., 2015). We found that *Meis2* mRNA levels in the OB of *Pbx1*Th animals were similar to those in controls (Fig. S5), suggesting that, analogous to what has been reported, PBX1 is not upstream of *Meis2* transcription but is required for MEIS2 protein stability.

PBX1 operates as olfactory bulb dopaminergic terminal selector

In different tissues and organisms, PBX and MEIS factors physically interact to co-regulate many target genes (Penkov et al., 2013). In mouse OB, PBX1 binds ∼3.5 kb upstream of the *Th* transcriptional start site, a region also bound by MEIS2 and which overlaps with a predicted DLX consensus site (Fig. 3A) (Agoston et al., 2014; Grebbin et al., 2016).

In *C. elegans*, CEH-20/PBX1, together with AST-1/ETV1 and CEH-43/DLX, directly bind and activate *cat-2/Th* expression (Doitsidou et al., 2013). Therefore, we investigated whether, in addition to binding near the MEIS2 and DLX sites, PBX1 also binds near the *in vivo* reported ETV1-binding site in the *Th* promoter region (Fig. 3A) (Cave et al., 2010; Flames and Hobert, 2009). Our ChIP qPCR analysis showed this to be the case (Fig. 3B) and suggested that PBX1, MEIS2, DLX and ETV1 could constitute a TF collective of DA terminal selectors similar to that described in *C. elegans* for CEH-20/PBX, AST-1/ETV1 and CEH-43/DLX (Doitsidou et al., 2013). Moreover, PBX1 binding to both proximal and distal sites suggests it might be necessary for the correct physical interactions of the *Th* enhancer and promoter.

Acting as terminal selectors, TFs work broadly to activate the expression of multiple genes that are necessary for neuron subtype-specific functions (Hobert, 2008). DA neurons are characterized by

Development (2020) 147, dev186841. doi:10.1242/dev.186841

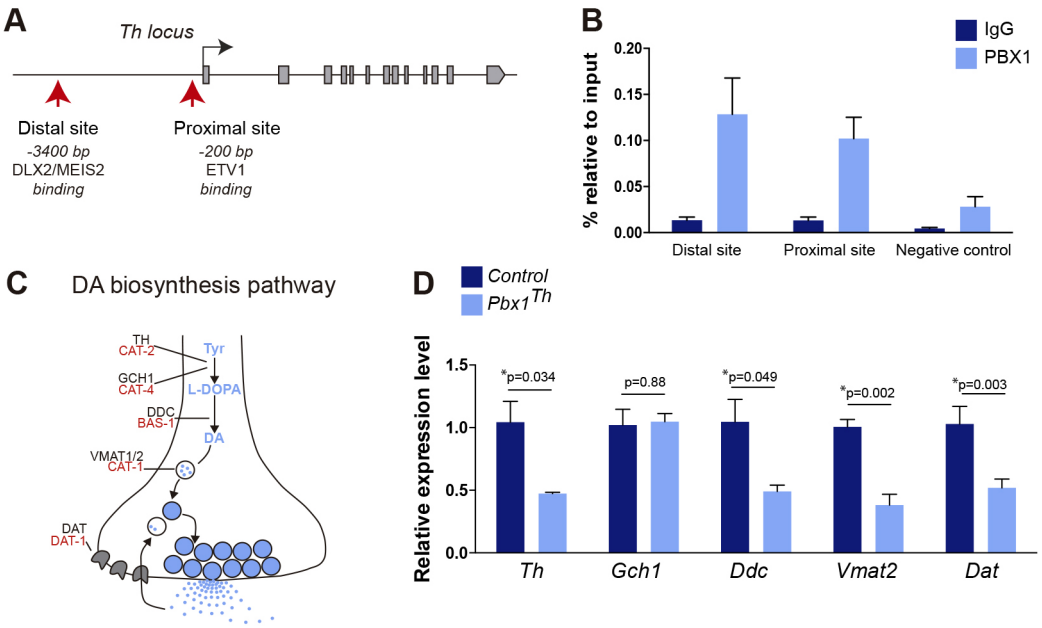

Fig. 3. PBX1 is a terminal selector for OB DA neuron fate. (A) Schematic representation of the tyrosine hydroxylase locus with binding sites for MEIS2, ETV1 and DLX. (B) ChIP qPCR from OB tissue shows PBX1 binding to both *Th* proximal and distal sites. PBX1-binding specificity was tested with the *untr17*-negative binding region. (C) Schematic representation of the conserved dopamine biosynthesis pathway. Mouse names are in black and *C. elegans* orthologs are in red. DA, dopamine; DAT/DAT-1, dopamine transporter; DDC/BAS-1, aromatic-L-amino-acid decarboxylase; GCH/1CAT-4, GTP cyclohydrolase; TH/CAT-2, tyrosine hydroxylase; Tyr, tyrosine; VMAT/CAT-1, vesicular monoamine transporter. (D) mRNA expression levels of dopamine pathway genes in controls and $Pbx1^{Th}$ mutants measured by qRT-PCR. n=4 animals (controls) $Pbx1^{Th}$ n=3 animals ($Pbx1^{Th}$), two-tailed unpaired Student's t-test. See Table S1 for the primary data for quantifications.

the expression of a battery of enzymes and transporters called the dopamine pathway genes, which allow for the synthesis and use of dopamine as neurotransmitter (Fig. 3C). In *C. elegans*, CEH-20/PBX acts as a DA terminal selector and is required for the correct expression of all dopamine pathway genes. Therefore, we next assessed the expression levels of dopamine pathway genes in $Pbx1^{Th}$ animals. The genes, *Ddc*, *Gch1*, *Vmat2* and *Dat*, are expressed at low levels in the OB compared with hypothalamic or midbrain DA populations, and are not detectable by immunohistochemistry or *in situ* hybridization staining (Weihe et al., 2006). These genes are uniquely expressed by DA neurons in the OB; thus, we quantified mRNA levels by qRT-PCR. As expected, $Pbx1^{Th}$ animals showed a significant decrease in *Th* mRNA level compared with control animals. In addition, *Ddc*, *Vmat2* and *Dat*, but not *Gch1*, were also significantly downregulated in $Pbx1^{Th}$ mutants (Fig. 3D; Table S1). Altogether, our data support a late role for PBX1 as a terminal selector for OB DA neuron fate; however, it remains to be determined whether PBX1, similar to its direct binding to *Th* regulatory regions, also directly binds to the regulatory regions of other dopamine pathway genes.

PBX1 directs morphological maturation of olfactory bulb dopaminergic neurons

For both *C. elegans* and mammals, it is well established that terminal selectors have a direct role on the transcriptional activation of neuron type-specific effector genes (Hobert, 2011). However, it is unclear whether they also play a role in the regulation of other cell maturation features, such as cellular morphology and axon projections. A few examples seem to indicate that this might be the case (Donovan et al., 2019; Lodato et al., 2014; Luria et al., 2008; Shirasaki et al., 2006); therefore, we next investigated the morphological maturation of OB DA neurons upon late deletion of *Pbx1*.

In the OB, DA somas surround the glomeruli that are invaded by DA dendritic projections (Fig. 4A; Kosaka and Kosaka, 2016). From our GFP lineage-tracing analysis, we noticed a general decrease in GFP labeling inside the glomeruli of $Pbx1^{Th}$ animals (Fig. 4B,C). Indeed, quantification of the area occupied by DA fibers revealed a significant decrease in GFP-positive pixels in $Pbx1^{Th}$ animals compared with controls (Fig. 4D; Table S1). As the number of GFP-positive cells surrounding the glomeruli (Fig. 1I; Table S1) and glomerulus area (Fig. 4D, Table S1) were not affected in $Pbx1^{Th}$ mutants, this difference is probably due to morphological defects of $Pbx1^{Th}$ DA neurons.

To directly study the cellular morphology of individual cells, we performed postnatal *in vivo* electroporations. SEZ progenitors of newborn control ($Pbx1^{+/+}$) and $Pbx1^{Fl/Fl}$ animals were co-electroporated with a plasmid expressing CRE recombinase under the *Th* promoter and a CRE-inducible GFP expression plasmid (Fig. 4E). Animals were sacrificed 31 days after electroporation to allow for the migration and maturation of electroporated cells. In control animals, 68% of GFP-expressing cells co-express TH, whereas in $Pbx1^{Fl/Fl}$ animals, only 44% of GFP cells are TH positive (Fig. 4F; Table S1). Therefore, these data confirm a late and cell-autonomous role for PBX1 in the induction of OB DA neuron differentiation. Morphological reconstruction of individual electroporated cells shows striking differences between control and $Pbx1^{Fl/Fl}$ animals (Fig. 4G). $Pbx1^{Fl/Fl}$-electroporated cells seem morphologically simpler and more immature than controls. They display a different branching distribution (Fig. 4H), significantly fewer primary dendrites (Fig. 4I), lower total dendrite length, lower dendrite volume, fewer branching points and a lower maximum cell radius (Fig. 4J; Table S1). Altogether, our data show that, in addition to its role in dopamine pathway gene activation, PBX1 is also required for the

Development (2020) 147, dev186841. doi:10.1242/dev.186841

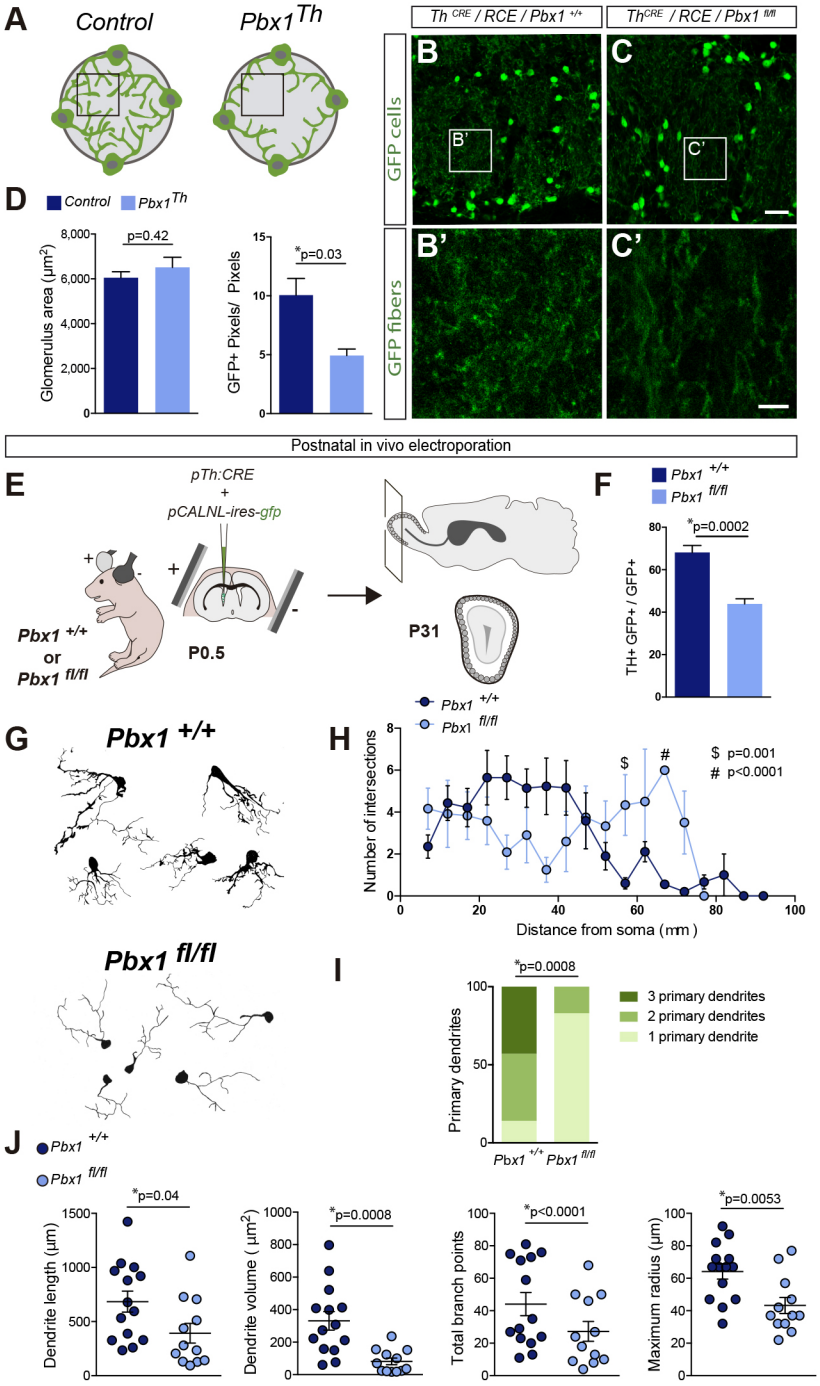

Fig. 4. PBX1 controls morphological maturation of olfactory bulb dopaminergic neurons. (A) Schematic representation of DA neurons surrounding OB glomerulus in controls and *Pbx1*Th mutants. (B-C′) DA lineage tracing from the RCE allele. Scale bars: 25 µm (B,C); 5 µm (B′,C′). (D) Quantification of glomerulus area and GFP fibers inside glomeruli of controls and *Pbx1*Th mutants. *n*=3 animals for each genotype, two-tailed unpaired Student's *t*-test. (E) Experimental design for postnatal *in vivo* electroporations. *Pbx1*$^{+/+}$ and *Pbx1*$^{fl/fl}$ animals are electroporated with a plasmid for expression of CRE recombinase under the control of the *Th* promoter and a floxed *gfp*-inducible plasmid. Mice are analyzed 31 days post-electroporation. (F) Induced deletion of *Pbx1* by *in vivo* electroporation leads to a decreased number of electroporated cells co-expressing TH. *n*=5 (*Pbx1*$^{+/+}$) and *n*=12 (*Pbx1*$^{fl/fl}$) electroporated animals, two-tailed unpaired Student's *t*-test. (G) Morphological reconstruction of electroporated cells in *Pbx1*$^{+/+}$ and *Pbx1*$^{fl/fl}$ animals. (H) Morphological Sholl analysis shows different branching distributions between *Pbx1*$^{+/+}$ and *Pbx1*$^{fl/fl}$ electroporated cells. *n*=14 cells from three animals (*Pbx1*$^{+/+}$) and *n*=12 cells from three animals (*Pbx1*$^{fl/fl}$), multiple two-tailed unpaired Student's *t*-test with Holm-Sidak adjusted *P*-value. (I) Frequency distribution of primary dendrites in *Pbx1*$^{+/+}$ and *Pbx1*$^{fl/fl}$ electroporated cells. *n*=14 cells from three animals (*Pbx1*$^{+/+}$) and *n*=12 cells from three animals (*Pbx1*$^{fl/fl}$), χ^2 test. (J) Morphological quantification of dendrite length, dendrite volume, branching points and maximum radius in *Pbx1*$^{+/+}$- and *Pbx1*$^{fl/fl}$-electroporated cells. *n*=14 cells from three animals (*Pbx1*$^{+/+}$) and *n*=12 cells from three animals (*Pbx1*$^{fl/fl}$), two-tailed unpaired Student's *t*-test, length, volume, radius, χ^2 branching points. See Table S1 for the primary data for quantifications.

morphological maturation of OB DA neurons, expanding the number of known roles for terminal selectors.

PBX1 is postmitotically required to repress alternative interneuron cell fates

OB DA interneurons use both dopamine and γ-aminobutyric acid (GABA) as neurotransmitters (Borisovska et al., 2013). Therefore, we next assessed whether PBX1 is also required for the expression of effector genes related to GABA metabolism. GABA is synthesized from glutamate by glutamate decarboxylase enzymes GAD1 (also called GAD67) or GAD2 (also called GAD65). GAD67 is the enzyme predominantly expressed by OB DA neurons (Kiyokage et al., 2010). Unexpectedly, *Pbx1*Th animals showed an increase in the number of DA lineage cells expressing GAD67 compared with controls (Fig. 5A-C; Table S1). This result suggests that PBX1 acts, at least to some extent, as a repressor of the GABAergic neuron fate.

In OB adult neurogenesis, different SEZ progenitors give rise to non-overlapping GABAergic interneuron populations (classified by TH, CR or CB expression) (Merkle et al., 2007). Expression analysis of non-DA interneuron markers in DA lineage cells of control and *Pbx1*Th animals showed a small but highly significant de-repression of CR in *Pbx1*Th mutant cells, whereas CB expression is not affected (Fig. 5D-I; Table S1). Thus, our results indicate that,

Development (2020) 147, dev186841. doi:10.1242/dev.186841

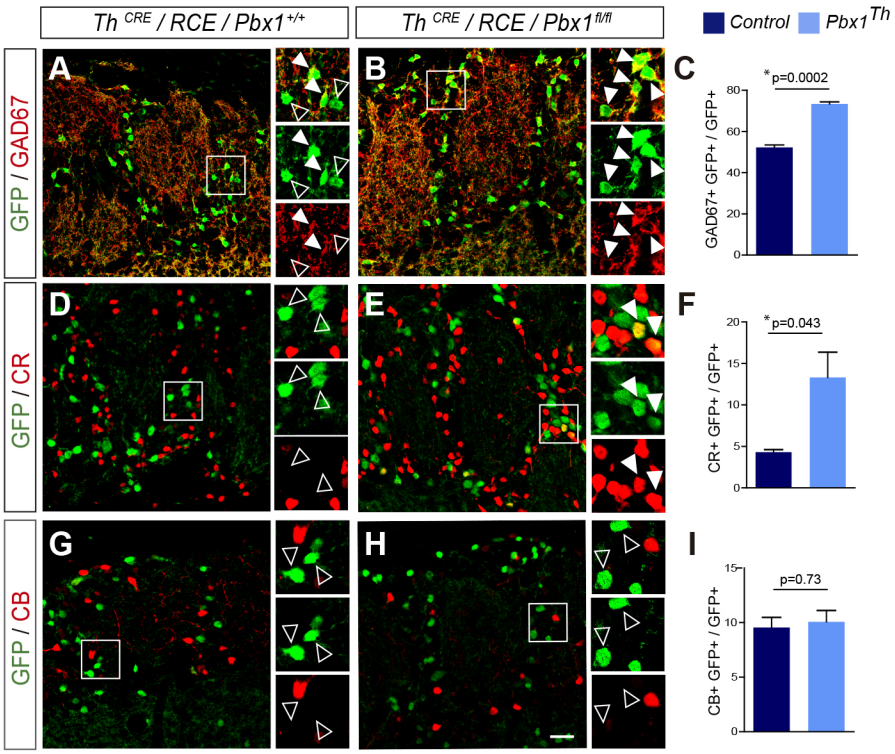

Fig. 5. PBX1 is required to repress alternative interneuron fates. (A,B) GAD67 expression in DA lineage cells of controls and *Pbx1*Th mutants. (C) Quantification of double GAD67- and GFP-positive cells. *n*=3 animals for each condition, unpaired two-tailed Student's *t*-test. (D,E) CR expression in the DA lineage cells of controls and *Pbx1*Th mutants. (F) Quantification of double CR- and GFP-positive cells. *n*=3 animals for each condition, unpaired two-tailed Student's *t*-test. (G,H) CB expression in the DA lineage cells of controls and *Pbx1*Th mutants. (I) Quantification of double CB- and GFP-positive cells. *n*=3 animals for each condition, unpaired two-tailed Student's *t*-test. Scale bar: 25 µm. See Table S1 for the primary data for quantifications. White arrowheads indicate colocalization; open arrowheads indicate lack of colocalization.

postmitotically, PBX1 is not only required for the correct expression of DA effector genes but also for repression of alternative cell fates. Interestingly, *C. elegans* terminal selectors are known to decrease cellular plasticity towards induced reprogramming by exogenous TFs (Patel and Hobert, 2017), which in more physiological conditions could be related to a role in restricting molecularly close and undesired cell fates.

Pbx1Th mutants show olfactory behavior deficits

Neuron-type differentiation defects are often translated into the inadequate execution of behaviors mediated by the corresponding neurons (Bacon et al., 2015; Chen et al., 2006; Erbel-Sieler et al., 2004; Liu et al., 2010). Although the specific functions of OB DA neurons are not well understood, they have been proposed to modulate odor detection, odor discrimination and gain control (Pignatelli and Belluzzi, 2017). Indeed, the activity of DA cells is directly proportional to odor concentration, and optogenetic silencing of these cells reduces mitral and tufted cell response to odors *in vivo* (Banerjee et al., 2015).

To analyze possible olfactory behavior impairments in *Pbx1*Th animals, we performed an odor threshold paradigm using increasing concentrations of a synthetic non-emotionally significant odor [geraniol ($C_{10}H_{18}O$)] (Fig. S6). Control animals can detect this odor at the lowest tested concentration (1 nM), whereas *Pbx1*Th mutants do not significantly react to this concentration (Fig. 6A; Fig. S6, Table S1). Odor behavioral defects of *Pbx1*Th mutants are not specific to geraniol as mutant animals also failed to detect carvone, an additional neutral odor, even at higher concentrations (13 nM) (Fig. 6B; Table S1). These results demonstrate the existence of odor detection defects in *Pbx1*Th animals.

In addition to expression in the OB, PBX1 is also expressed in midbrain DA neurons. Loss of *Pbx1* in this DA population is offset by the upregulation of *Pbx3* (Villaescusa et al., 2016); thus, midbrain DA neurons are unaffected in *Pbx1*Th, whereas double *Pbx1*Th/*Pbx3* mutants show midbrain DA neurodegeneration (Villaescusa et al., 2016). Nevertheless, we analyzed locomotion activity in *Pbx1*Th single mutants to discard the possibility that the observed odor impairments were due to underlying motor defects. Importantly, performance on the pole test (T-down), a paradigm used to evaluate midbrain DA neuron dysfunction, such as nigrostriatal projection deficits, was similar in *Pbx1*Th mutants and controls (Fig. 6C; Table S1).

Additional behavioral tests were performed to assess locomotion and anxiety in *Pbx1*Th mutants. Motor behavior measured in the open field test by total distance travelled and mean speed showed no differences between experimental groups (Fig. 6D; Table S1). Anxious behavior was analyzed by comparing time and number of entries in the center with the periphery of the open field. Statistical analyses of these variables in *Pbx1*Th mutants presented no differences compared with controls (Fig. 6D; Table S1). Finally, in order to evaluate a possible anxious interaction with novel objects, we used the marble-burying test, which is a measure of stereotypical behavior associated with anxiety and obsessive-compulsive disorder. We did not observe differences in the number of buried marbles between animal groups (Fig. 6E; Table S1). Thus, this test, along with the open-field results, suggests *Pbx1*Th exhibit normal anxiety levels.

In summary, we find that *Pbx1*Th defects in OB DA specification leads to odor impairments, whereas motor function or anxiety levels are unaffected.

Pbx1 splicing is dynamically regulated throughout olfactory bulb adult neurogenesis

Our results, together with previous reports, assign diverse functions to PBX1 throughout the SEZ adult neurogenic process. In progenitors, PBX1 controls neurogenic versus oligogenic commitment (Grebbin et al., 2016). Later, it is required for the survival of migrating neuroblasts (Grebbin et al., 2016) and, here, we show that during terminal differentiation, it acts as a terminal selector that induces DA neuron fate, morphological maturation and postmitotically restricting alternative cell fates. Therefore, we wondered how the plethora of PBX1 functions is temporally regulated as the cell ages.

Development (2020) 147, dev186841. doi:10.1242/dev.186841

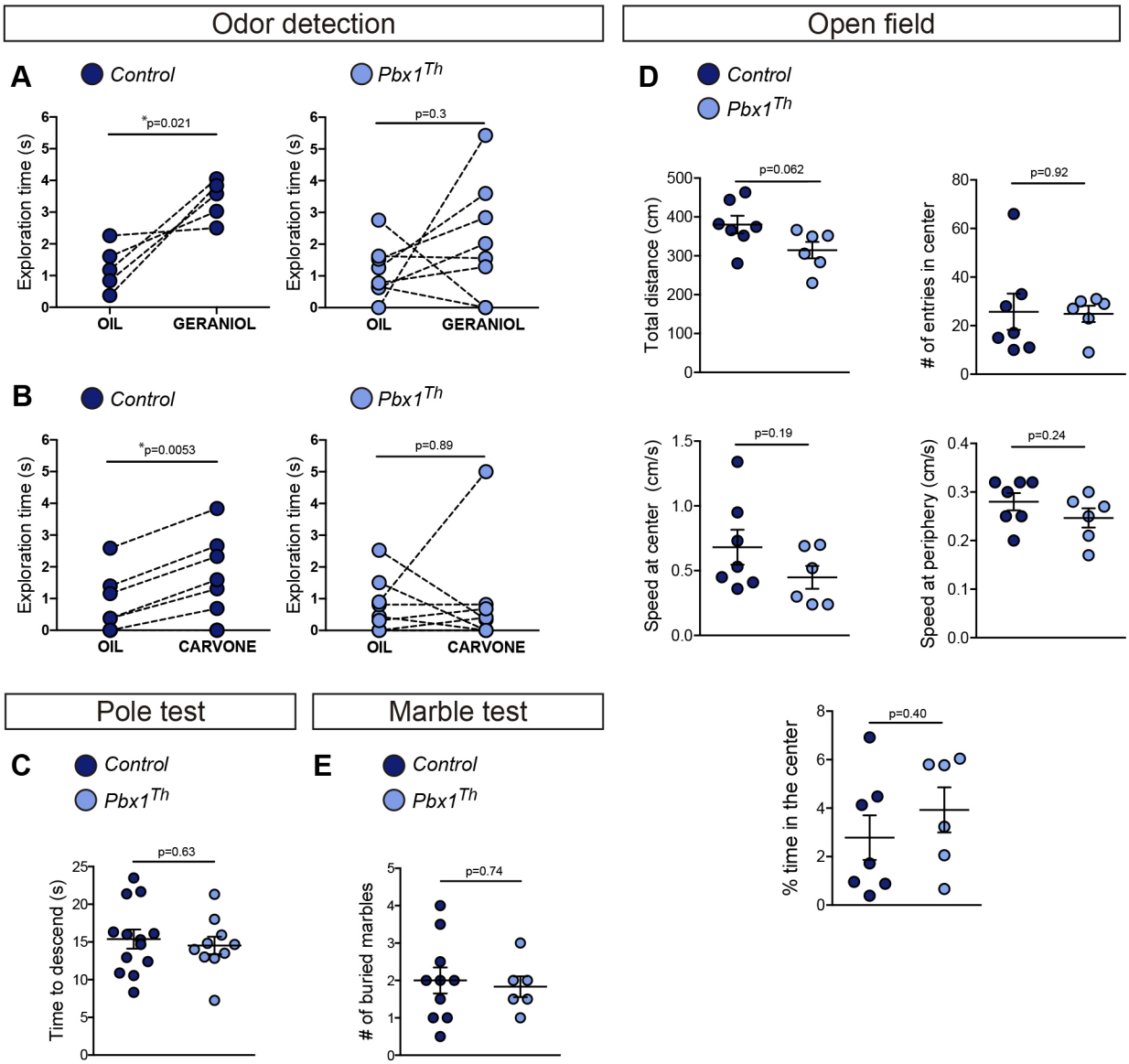

Fig. 6. *Pbx1*Th mutants show olfactory behavioral deficits. (A,B) Quantification of the exploration time for two neutral odors, geraniol and carvone, in controls and *Pbx1*Th mutants, paired two-tailed *t*-test. (C) Pole-test results. Quantification of the time required to descend from a vertical pole in controls and *Pbx1*Th mutants, unpaired two-tailed *t*-test. (D) Analysis of the motor behavior displayed in an open field by controls and *Pbx1*Th mutants, unpaired two-tailed *t*-test. (E) Quantification of the number of buried marbles by controls and *Pbx1*Th mutants, unpaired two-tailed *t*-test. See Table S1 for the primary data for quantifications and Fig. S6 for geraniol threshold determination in controls and *Pbx1*Th mutants. Data points represent individual values for each animal; data points linked by a dashed line represent the same animal tested under two different conditions.

Specific PBX1 functions could be modulated by unique cellular contexts (e.g. the presence of different cofactors at each stage). However, like *Pbx1*, other TFs involved in OB DA neuron differentiation, such as *Dlx2*, *Pax6*, *Etv1*, *Meis2* and *Coup-tf1*, are also expressed at earlier stages of differentiation (Agoston et al., 2014; Brill et al., 2008; de Chevigny et al., 2012; Flames and Hobert, 2009; Zhou et al., 2015). Recently, alternative splicing has been demonstrated to be very prevalent in the nervous system where it provides increased functional diversity to proteins with important neuronal functions (Furlanis and Scheiffele, 2018; Vuong et al., 2016). Therefore, we aimed to explore whether alternative splicing could be involved in controlling the functional switching of PBX1.

The *Pbx1* gene can generate three different coding isoforms that differ in their C-terminal domain (Fig. 7A). *Pbx1a*, the longest isoform (coding for PBX1a, 430 amino acids), includes all coding exons. The *Pbx1b* isoform skips exon 7, leading to a shift in the open reading frame and coding for a shorter protein with a different C-terminal domain (PBX1b, 347 amino acids). Finally, *Pbx1c* skips exons 6 and 7, and gives rise to a truncated version of PBX1a (PBX1c, 339 amino acids) (Fig. 7A). Using specific antibodies against PBX1a and PBX1b isoforms we found that both isoforms are expressed in the adult OB (Fig. 7A-D). PBX1c isoform expression was not analyzed due to a lack of specific antibodies. Interestingly, double immunoanalysis with TH reveals that all DA cells express PBX1a whereas PBX1b expression is absent (Fig. 7E-G). Next, we analyzed PBX1 isoform expression at earlier stages of differentiation. As opposed to mature DA neurons, almost all SEZ cycling progenitors (labeled by Ki67 expression) express PBX1b but lack PBX1a isoform expression (Fig. 7H-J). Finally, immature migrating neuroblasts in the SEZ and RMS labeled with DCX,

Development (2020) 147, dev186841. doi:10.1242/dev.186841

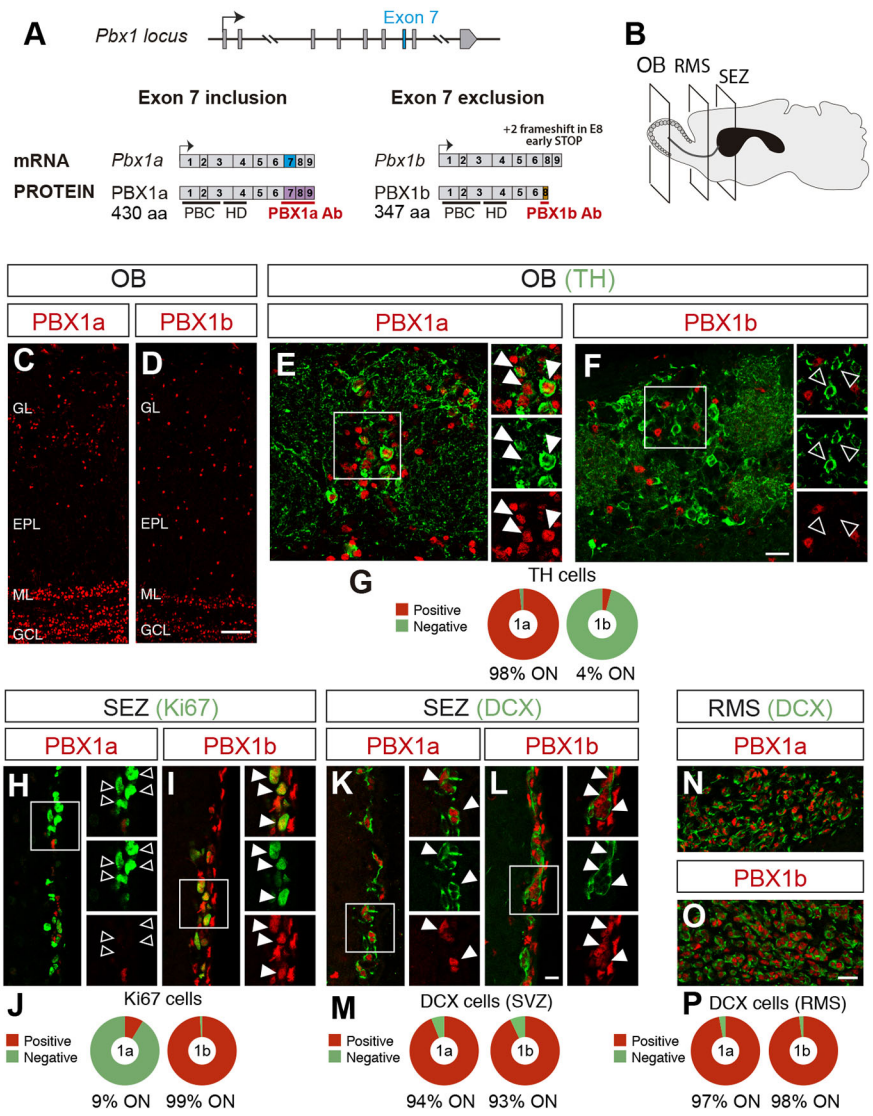

Fig. 7. *Pbx1* exon 7 skipping is tightly regulated throughout the OB DA neurogenic process. (A) Schematic representation of the *Pbx1* locus and the isoforms generated by alternative splicing of exon 7 (in blue). The black bars indicate the location of the DNA-binding domains and the red bars represent the domain recognized by the isoform-specific antibodies. Purple and orange boxes in the protein coding regions represent amino acid differences between the two isoforms. Ab, antibody; HD, homeodomain DNA binding domain, PBC, PBC DNA-binding domain. (B) Brain representation of the coronal levels analyzed in the micrographs. OB, olfactory bulb; RMS, rostral migratory stream; SEZ, subependymal zone. (C,D) Analysis of PBX1a and PBX1b expression in the adult OB with isoform-specific antibodies. Scale bar: 75 µm. EPL, external plexiform layer; GCL, granular cell layer; GL, glomerular cell layer; ML, mitral cell layer. (E,F) Double immunostaining of TH with PBX1a and PBX1b antibodies. Scale bar: 25 µm. (G) Quantification of PBX1a and PBX1b expression in OB DA cells. (H,I) Analysis of PBX1a and PBX1b expression in SEZ proliferating progenitors labeled with Ki67 antibody. (J) Quantification of PBX1a and PBX1b expression in SEZ proliferating cells. (K,L) Analysis of PBX1a and PBX1b expression in SEZ migrating neuroblasts labeled with DCX antibody. Scale bar: 10 µm. (M) Quantification of double immunostaining of DCX with PBX1a and PBX1b isoforms in SEZ. (N,O) Analysis of PBX1a and PBX1b expression in RMS migrating neuroblasts labeled with DCX antibody. Scale bar: 20 µm. (P) Quantification of double immunostaining of DCX with PBX1a and PBX1b isoforms in RMS. White arrowheads indicate colocalization; open arrowheads indicate lack of colocalization.

co-express both PBX1b and PBX1a isoforms (Fig. 7K-P). In conclusion, our analysis reveals a temporal gradient of exon 7 inclusion throughout the adult DA neurogenic process: progenitors skip exon 7 but it is partially included in migrating neuroblasts and is always present in mature DA neurons.

The long PBX1 isoform specifically rescues dopaminergic terminal differentiation defects of *Pbx1*Th mutant mice

PBX TFs are evolutionarily ancient and present in different animal groups including bilateria and cnidaria. Sequences homologous to mouse exon 7 are present in all *Pbx1* vertebrate genes but they are absent in invertebrates. Importantly, exon 7 is alternatively spliced in fish, frogs, mice and humans, suggesting that this splicing event bears important functions (Fig. 8A). Analysis from available expression data for *Pbx1* exon 7 inclusion throughout mouse and human brain development (Tapial et al., 2017) shows that exon 7 is mostly excluded from mouse neuronal progenitors and at the earliest stages of human forebrain development, and it is progressively included during brain development, being the predominant isoform at the end of cortical neurogenesis (Fig. 8B). Additionally, it has been reported that, *in vitro*, mouse embryonic stem cells mostly skip exon 7, and forced expression of the long-isoform *Pbx1a* induces aberrant transcription of neuronal genes (Linares et al., 2015).

In light of the phylogenetic conservation of exon 7 alternative splicing, its increased inclusion during brain development in mice and humans, and its tight temporal control in adult SEZ neurogenesis, we explored whether PBX1a and PBX1b isoforms are functionally different *in vivo*. To this end we performed electroporations of CRE recombinase under the control of the *Th* regulatory region on *Pbx1*$^{Fl/Fl}$ and expressed GFP alone, or GFP plus each *Pbx1* isoform (Fig. 8C). As we previously described, late deletion of *Pbx1* by CRE electroporation leads to defects in TH expression (Fig. 8D,G; Table S1). Importantly, these TH-expressing defects could be rescued by co-electroporation of an inducible *Pbx1a*-expressing construct but not through *Pbx1b* expression (Fig. 8E-G; Table S1), which suggests that the 97 amino acid C-terminal domain of PBX1a confers specific functions to PBX1 for the induction of dopaminergic neuron fate.

DISCUSSION

PBX1 acts as terminal selector for olfactory bulb dopaminergic neuron fate

Here, we show that *Pbx1* is expressed throughout the OB DA neurogenic process from progenitors to differentiating neurons, and its expression is maintained throughout the life of the OB DA cells. In

Development (2020) 147, dev186841. doi:10.1242/dev.186841

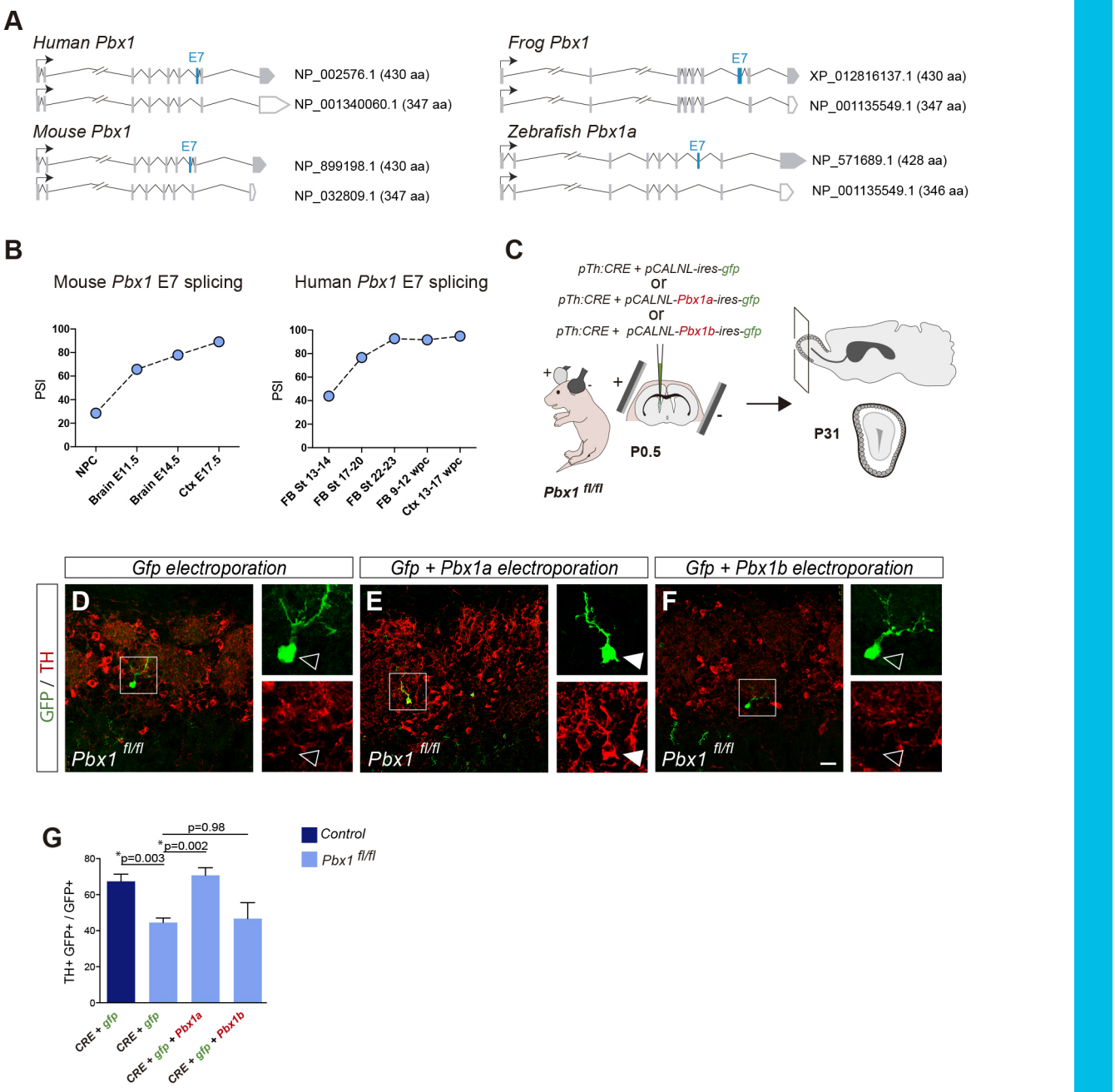

Fig. 8. The long *Pbx1* isoform specifically rescues DA terminal differentiation defects of *Pbx1*Th mutants. (A) Representation of *Pbx1* exon 7 alternative splicing isoforms that are present in human, mouse, frog and zebrafish. (B) Percent spliced-in (PSI) values for *Pbx1* exon 7 throughout mouse and human neurodevelopmental progression. Data source: VastDB (Tapial et al., 2017). Ctx, cortex; E, embryonic day; FB, Forebrain; NPC, neuronal precursor; St, Carnegie stage; wpc, weeks post-coitum. (C) Schematic representation of the experimental design. *Pbx1*$^{fl/fl}$ mutant animals are electroporated with a plasmid for CRE recombinase expression under the *Th* promoter and a *Gfp*, *Gfp+Pbx1a* or *Gfp+Pbx1b* inducible plasmid. Mice are analyzed 31 days post-electroporation. (D-F) Representative pictures of electroporated GFP cells and TH expression under the different experimental conditions. Scale bar: 20 µm. (G) Quantification of TH expression in the electroporated cells. Tukey's multiple comparison test. See Table S1 for the primary data for quantifications.

addition to its known early roles in neurogenesis and neuroblast survival (Grebbin et al., 2016), late depletion of *Pbx1* in maturing DA neurons allowed us to unravel its role in DA terminal differentiation. PBX1 is required for the expression of a broad range of OB DA effector genes, and we determined that, at least for *Th*, this regulation is direct. Moreover, PBX1 is not required for the transcription of other TFs known to be necessary for OB DA specification, although it seems to stabilize MEIS2 protein, as determined in other systems (Dardaei et al., 2014; Garcia-Cuellar et al., 2015). Altogether, our data suggest that PBX1 acts as a terminal selector for OB DA neuron fate. Interestingly, PBX1 is also required for midbrain DA neuron specification (Villaescusa et al., 2016). However, the regulatory program controlling midbrain DA neuron specification is not shared with the OB, as a different set of TFs control midbrain DA neuron specification (Flames and Hobert, 2011) and in this brain region PBX1 acts as an upstream regulator of *Pitx3*, a TF that acts as midbrain DA terminal selector. Thus, PBX1 seems to act at different levels in OB and midbrain DA neuron specification.

Development (2020) 147, dev186841. doi:10.1242/dev.186841

Neuron morphology and alternative fate repression are also part of the terminal selector regulatory program

Previous studies in *C. elegans* have established that terminal selectors directly bind and activate expression of neuron type specific effector genes (Hobert, 2011). However, it is unclear whether these TFs play additional roles in neuron-type specification programs. Here, we show that PBX1 is terminally required for correct morphological maturation of OB DA cells, expanding the known functions of terminal selectors. Currently, effector genes controlling OB DA neuron morphology are unknown. Interestingly, PBX1a is required for correct axon pathfinding in midbrain DA neurons through regulation of the netrin receptor DCC (Sgadò et al., 2012). It would be interesting to determine whether DCC signaling is also involved in correct OB DA morphology and whether DCC expression in the OB is regulated by PBX1.

In addition to this unforeseen role of PBX1 as a morphological determinant, we also find that postmitotic removal of PBX1 leads to de-repression of effector genes from other cell lineages, implying that terminal selectors are also actively involved in restraining alternative cell fates. Of note, other TFs required in OB terminal differentiation programs show similar dual roles as activators and repressors of specific cell fates. For example, expression of a dominant-negative form of *Meis2* leads to a decrease in TH expression accompanied by induction of CR expression (Agoston et al., 2014). This phenotype, which is very similar to the Pbx^{Th} phenotype, also supports the function of MEIS2/PBX1 as a complex. Complementarily, deletion of *Sp8* or *Zic1/2*, TFs that are expressed in the CR lineage, leads to defects in CR expression and ectopic TH induction (Gaborieau et al., 2018; Tiveron et al., 2017). Repression of alternative fates might be an important function of some terminal selectors. In line with this hypothesis, a recent report shows that *unc-3*, a terminal selector for *C. elegans* motorneuron specification, also acts as a repressor of alternative neuronal fates (Feng et al., 2020).

In *C. elegans*, terminal selectors restrain neuronal plasticity to induced reprogramming, at least in part, through epigenetic mechanisms (Patel and Hobert, 2017). Future experiments should determine whether DA cells lacking *Pbx1* have defects in chromatin compaction, and whether those defects are responsible for ectopic CR expression.

Neuron-subtype terminal differentiation programs are phylogenetically conserved

In *C. elegans*, CEH-20/PBX1, AST-1/ETV1 and CEH-43/DLX2 are terminal selectors of DA neuron fate (Doitsidou et al., 2013; Flames and Hobert, 2009). Our characterization of PBX1 as a DA terminal selector, along with previous reports on ETV1 and DLX2 roles in OB DA terminal differentiation (Brill et al., 2008; Cave et al., 2010; Flames and Hobert, 2009), suggest that these two neuronal populations in *C. elegans* and mammals share the same terminal regulatory program. As previously mentioned, mouse *Pax6*, *Meis2* and *Coup-tf1* TFs are also involved in OB DA terminal differentiation. Our own unpublished results in *C. elegans* indicate that nematode orthologs for these TFs (*vab-3*, *unc-62* and *unc-55*, respectively) are also necessary for correct DA specification in the worm (A. Jimeno and N.F., unpublished). Altogether, these data indicate that nematode DA neurons and mammalian OB DA neurons share deep homology. Deep homology refers to the relationship between cells or structures in distant species that share their genetic regulatory programs. This concept has been previously proposed for other neuronal types in distant animals (Denes et al., 2007; Lloret-Fernández et al., 2018; Nomaksteinsky et al., 2013; Tomer et al., 2010). Indeed, the identification of homologous gene regulatory networks is an emerging strategy used to assign homologous neuronal types in distant species (Arendt, 2008; Arendt et al., 2019, 2016).

Temporal diversification of transcription factor functions through splicing regulation

TFs are usually broadly expressed, and it is well established that they fulfill different functions depending on their specific cellular contexts. Interactions with other differentially expressed TFs, as well as available chromatin landscapes, are thought to determine context-specific targets of a given TF (Reiter et al., 2017). However, TFs display different functions not only in distinct cell types but also throughout the differentiation of the same cell. In this context, cells have to rapidly transition from one regulatory state to another. These transitions imply the rapid rewiring of the transcriptional regulatory landscape of the cell (Rhee et al., 2016). How the same TFs dynamically switch their functional targets in a quick and efficient manner is currently poorly understood. Here, we show that regulation of TF alternative splicing could be an important mechanism controlling temporal modulation of TF functions.

Indeed, alternative splicing is more prevalent in TFs than in the rest of the genome, and defects in TF isoform expression may underlie multiple neurodevelopmental disorders (Porter et al., 2018). Despite evidence supporting the biological relevance of TF alternative splicing in nervous system development, very little is known about the functional differences between splicing variants of the same TF (Bohrer et al., 2015; Huynh et al., 2011; Gabut et al., 2011; Pfurr et al., 2017; Raj et al., 2011; Rhee et al., 2016). Here, we provide an additional example of the diverse functionality of TF isoforms. More importantly, this is, to our knowledge, the first reported example of dynamic regulation of TF actions throughout neuronal development by alternative splicing.

How diverse actions of PBX1 isoforms are modulated remains to be determined. PBX1a and PBX1b isoforms share the homeodomain and PBC DNA-binding domains, suggesting their different actions are likely mediated through differential protein-protein interactions. Indeed, cell lines with different percentages of *Pbx1* exon 7 inclusion show broadly similar PBX1 DNA-binding profiling (Linares et al., 2015), and in SEZ and *in vitro* adult neural stem cells, PBX1 is already bound to *Th* even though the gene is still not expressed (Grebbin et al., 2016).

In summary, our results suggest that temporal control of TF alternative splicing could be used to diversify TF targets at various stages of neuron specification. It will be important in the future to investigate whether this is a widespread mechanism used to regulate the rapid rewiring of transcriptional regulatory programs that is required in the cell-state transitions taking place in the development of many tissues and organs.

MATERIALS AND METHODS

Animals

The generation and genotyping of $Pbx1^{Flx/Flx}$ conditional and *Pbx2* knockout mutant mice has been described previously (Koss et al., 2012; Selleri et al., 2004). Both strains were kindly provided by Dr Licia Selleri (University of California San Francisco, CA, USA). Th-IRES-Cre [B6.129X1-$Th^{tm1(cre)Te/Kieg}$] and RCE [Gt(ROSA)26$Sor^{tm1.1(CAG-EGFP)Fsh/Mmjax}$] mice were obtained from the European Mutant Mice Association (EM ID: 00254) and the Jackson Laboratory (stock number 32037-JAX), respectively. Both strains were genotyped as described previously (Lindeberg et al., 2004; Sousa et al., 2009). $Pbx1^{Fl/Fl}$ or $Pbx1^{+/+};Th^{CRE}$ animals were used as controls as no significant differences were found between these two genotypes. Housing and experiments were carried out following protocols approved by the ethics

Development (2020) 147, dev186841. doi:10.1242/dev.186841

committee of the Consejo Superior Investigaciones Científicas (Madrid, Spain) and in accordance with Spanish and European regulations.

For BrdU labeling, 8-week old male mice received seven intraperitoneal injections of 50 mg/kg body weight BrdU, one every 2 h, and were sacrificed 42 days after the last injection.

Histological analysis

Adult male mice were deeply anesthetized (5.5 µl/g of Dolethal) and transcardially perfused with 4% paraformaldehyde (PFA) in 0.1 M phosphate-buffered saline (PBS) (pH 7.4). Postnatal day (P) 0 pups were anesthetized by hypothermia before transcardial perfusion. Brains were dissected and postfixed by immersion in the same fixative overnight (o/n), washed in PBS for 2 h, cryoprotected o/n in 30% sucrose in PBS (w/v), mounted in OCT Compound (Aname) and serially sectioned (10 µm) using a Leica CM1900 cryostat. For morphology analysis, we obtained 50 µm floating sections with a sliding microtome (Leica SM2010R). Frozen sections were incubated for 1 h at room temperature in blocking buffer [0.1 M PBS containing 1% bovine serum albumin (v/v) and 0.2% Triton X-100 (v/v)]. For BrdU immunodetection, sections were first treated with 2 N HCl for 20 min at 37°C and neutralized in 0.1 M borate buffer (pH 8.5) for 10 min. For antigen retrieval, sections were boiled in 10 mM sodium citrate (pH 6), for 5 min and allowed to cool down slowly. Blocked sections were incubated o/n at 4°C with primary antibodies diluted in blocking buffer. Antibodies used were as follows: rabbit anti-TH (1:1000; Pel-Freez, P40101-0); mouse anti-TH (1:500; Millipore, MAB318); sheep anti-TH (1:1000; Pel-Freez, P60101-0); mouse anti-PBX1a (1:200; Santa Cruz Biotechnology, sc-101851); mouse anti-PBX1b (1:100; Santa Cruz Biotechnology, sc-101852); mouse anti-PBX2 (1:100; Santa Cruz Biotechnology, sc-890); rat anti-BrdU (1:400; Abcam, ab6326); rabbit anti-CR (1:2000; Millipore, MAB1568); rabbit anti-CB (1:2000; Swant, CB38); mouse anti-CR (1:3000; Millipore, MAB5054); chicken anti-GFP (1:1000; Aves Labs, GFP-1020); mouse anti-GAD67 (1:500; Millipore, MAB5406); mouse anti-MEIS2 (1:1000; Sigma-Aldrich, AV34684); mouse anti-COUP-TF1 (1:500; Persus Proteomics, H8132); rabbit anti-ER81 (1:1000, kindly provided by T. Jessel, Columbia University, NY, USA); and rabbit anti-PAX6 (1:1000; Developmental Studies Hybridoma Bank, AB-528427). After several PBS washes, the sections were incubated for 1 h at room temperature with Alexa Fluor 488-, Alexa Fluor 555- or Alexa Fluor 647-conjugated appropriate secondary antibodies (A21202, A21206, A31572, A31571, A21447, A21071, 1:600, Thermo Fisher Scientific) (1:600, Thermo Fisher Scientific). Samples were counterstained with 2-(4-amidinophenyl)-1H-indole-6-carboxamidine (DAPI, 0.4 mg/ml, Sigma-Aldrich), dehydrated in an ascending series of ethanols and mounted with Entellan (Millipore).

For quantification of BrdU-labeled cells, samples were analyzed using a Zeiss ImagerM2 microscope. All BrdU-positive cells of the entire glomerular cell layer were counted in 16 sections along the entire rostro-caudal extent of the olfactory bulb. No fewer than 100 BrdU-positive cells per animal were scored. For quantifications of TH-positive cells (P0 and adult animals), GFP-positive cells and colocalization in immunofluorescence, samples were analyzed with a TCS-SP8 Leica Microsystems confocal microscope. For OB quantification, dorsal, ventral, medial and lateral regions of the glomerular cell layer were randomly sampled with a predetermined area (184×184 µm corresponding to the field at 63× magnification) and all immunopositive cells in these selected areas were counted. In all cases, cells were sampled from six sections along the rostro-caudal axis of the olfactory bulb. A minimum of 400 GFP-positive cells per animal were scored. To analyze the *in vivo* electroporations, all GFP-positive cells of the glomerular cell layer were counted in every fourth section. A minimum of 100 GFP-positive cells per animal were analyzed. For expression analysis of PBX1a and PBX1b in the SEZ, five sections covering the extent of the SEZ per animal were analyzed. For the analysis of the amount of Ki67-positive cells and DCX-positive cells per area, a minimum of three sections were analysed, corresponding to at least 300 Ki67-positive cells and 400 DCX-positive cells.

Behavioral tests

Male animals between 8 and 12 weeks old were used. Olfactory threshold detection method was run as described previously (Perez-Villalba et al., 2018). Briefly, mice were placed in a 22.5 cm^2 open Plexiglas box with chip bedding. After 3 min of exploration, a cotton stick soaked in non-odorant mineral oil was introduced into the box through a 1 cm diameter hole. The stick was presented for 1 min and thereafter substituted by a series of five consecutive fresh cotton sticks also soaked in non-odorant mineral oil to produce habituation to the novel stimulus. Mice were then exposed for 1 min to successive cotton sticks with 3:1 increasing concentrations of geraniol ($C_{10}H_{18}O$; Ventós) diluted in mineral oil: 1 nM, 3 nM, 11 nM, 36 nM, 111 nM and 341 nM. A different set of animals was exposed to carvone ($C_{10}H_{14}O$, Sigma-Aldrich) at 13 nM, after stick habituation. Carvone vapor pressure is slightly higher than geraniol (0.115 mmHg and 0.03 mmHg, respectively at 25°C); thus, at the same concentration, more volatile carvone is available. Nevertheless, to ensure values above detection threshold, we used 13 nM carvone instead of the 1 nM used for geraniol. Olfactory exploration and subsequent behavioral experiments were recorded and tracked with Smart Video Tracking Software (Panlab). After each test, behavioral instruments were thoroughly wiped clean with 70% alcohol.

In the open-field test, general locomotor activity was examined in a 40 cm^2 gray squared box (Panlab). Mice were carefully introduced into the open field and recorded for 20 min. Periphery/center areas were automatically established by the Smart video tracking software (Panlab, Harvard Apparatus). Variables, such as mean speed (cm/s), total distance traveled (cm), time in areas and number of entries, were analyzed.

In the marble-burying test, mice were placed for 10 min in a clean home cage with four small crystal marbles randomly distributed. The number of totally buried marbles (1 point) or half-buried marbles (0.5 points) was measured.

For pole-test analysis, each mouse was placed head upwards on top of a wooden pole (1 cm diameter and 45 cm long). When placed on the pole, the mouse self-oriented downwards and descended the pole. The time between the placement on pole and the moment when the four paws touched the floor (T-down) was measured, with a time limit of 90 s. All experimental subjects were tested for three trials and the time average was considered for representation.

In vivo electroporations

The SEZ electroporation procedure was based on published methods (Boutin et al., 2008; Fernández et al., 2011). Briefly, P0 male and female mice were anesthetized by hypothermia, fixed on a custom-made support plate placed in a stereotaxic rig and injected at the midpoint of a virtual line connecting the eye with the cranial landmark Lambda with hand-pulled glass pipettes. Plasmid solution (0.8 µl) was injected in combination with 1% Fast Green (Sigma-Aldrich). The accuracy of the injection could be monitored by the filling of the injected ventricle by the dark solution. Only successfully injected mice were subjected to five electrical pulses (135 V, 50 ms pulse and 950 ms intervals) using the ECM 830 BTX electroporator (Harvard Apparatus) and tweezer-style reusable electrodes. Electroporated animals were reanimated for several minutes on a 37°C heating plate before being returned to the mother.

Plasmids used in this study were prepared by using an EndoFree Plasmid Maxi Kit (Qiagen) and resuspended in sterile PBS at a final concentration of 4-6 µg/µl. pTh:CRE plasmid (pNF365) was built with a CRE sequence from the pCAG-Cre backbone (Addgene, 26647) replacing the luciferase sequence in the TH5kb_pGL3 plasmid (Flames and Hobert, 2009). pCALNL-IRES-EGFP (pNF320), was built by replacing the DsRed sequence of pCALNL-DsRed plasmid (Addgene, 13769) with an 'IRES-EGFP' cassette from pCAGIG (Addgene, 11159). *Pbx1a* and *Pbx1b* were then cloned into pCALNL-IRES-EGFP to generate pNF419 and pNF420, respectively.

Morphology measurements

For fiber analysis, GFP levels were measured after anti-GFP immunostaining. The inner contour of 26 glomeruli per animal (at 63× magnification) was delimited and the area was analyzed using ImageJ. After background analysis, the threshold for minimal GFP-positive pixel value was set to 20. Results are expressed as percentage of GFP-positive pixels with respect to the total number of pixels in the area.

To analyze the morphology of electroporated neurons, randomly selected GFP-positive neurons in the OB glomerular layer of $Pbx1^{+/+}$ and $Pbx1^{Flx/Flx}$ were photographed at 63× magnification using a TCS-SP8 Leica confocal

Development (2020) 147, dev186841. doi:10.1242/dev.186841

microscope, and maximum projections from image *z* stacks (every 0.75 µm) were generated. GFP cells were confirmed PBX1a and TH positive in $Pbx1^{+/+}$electroporated animals, and PBX1a negative and TH negative in $Pbx1^{Flx/Flx}$ electroporated animals. In both genotypes, for each neuron, different morphometric parameters were measured using the NeuronStudio software package.

ChIP PCR

For the ChIP assay, the olfactory bulbs of three C57Bl/6 adult male animals (8-12 weeks old) were dissected for each experiment. The tissue was dissociated in papain solution at 37°C for 50 min followed by Dounce homogenization. Cells were fixed in 1% formaldehyde (Sigma-Aldrich) for 15 min. Fixed cells were washed with PBS and lysed in lysis buffer [NaCl 0.1 M, Tris-HCl 50 mM (pH 8), EDTA 5 mM and 0.5% SDS] (1 ml/10^7 cells) at 4°C for 10 min. After centrifugation, the pellet was resuspended in two parts of lysis buffer and one part of triton buffer [NaCl 0.1 M, Tris-HCl 0.1 M (pH 8), EDTA 5 mM and 0.5% Triton X-100]. Cell lysates were sonicated using a Bioruptor (Diagenode) for five cycles (30 s ON/30 s OFF). The PBX1 antibody (2 µg, Cell Signaling Technology, 4342) was incubated with 30 µl of Dynabeads Protein G (Invitrogen) o/n at 4°C. The antibody was then added to the chromatin solution, which was diluted 2:1 in dilution buffer [1.1% Triton X-100 , EDTA 1.2 mM, Tris-HCl 16.7 mM (pH 8) and NaCl 167 mM] and incubated o/n at 4°C. Immune complexes were washed twice with low salt buffer [0.1% SDS, 1% Triton X-100, 2 mM EDTA, 20 mM Tris-HCl (pH 8) and 150 mM NaCl] twice with high salt buffer [0.1% SDS, 1% Triton X-100, 2 mM EDTA, 20 mM Tris-HCl (pH 8) and 500 mM NaCl] once with LiCl immune complex buffer [LiCl 0.25 M (Sigma-Aldrich), 1% NP40 (Sigma-Aldrich), 1% deoxycholic acid, 1 mM EDTA and 10 mM Tris-HCl (pH 8)] and twice with TE buffer [1 mM EDTA and 10 mM Tris-HCl (pH 8)]. Finally, DNA was eluted in 20 µl 10% SDS, 20 µl 1 M $NaHCO_3$ and 160 µl of double distilled H_2O per sample. Crosslinks were reversed at 65°C o/n, proteins were digested using proteinase K, and DNA was purified using the QIAQUICK PCR Purification Kit (Qiagen). Quantitative RT-PCR was performed with Fast SYBR Green (Applied Biosystems) in a 7500 Fast Real-Time PCR System (Applied Biosystems). The percentage of input is represented, showing the amount of DNA pulled down using the antibody of interest in the ChIP reaction, relative to the amount of starting material (input sample). The following formula was used $(2^{-(\text{sample Ct}-\text{INPUT Ct})}\times 100)/3000$ (3000 corrects the dilution factor). Normal rabbit IgG (Santa Cruz Biotechnology, sc-2027) was used as a negative control for the nonspecific binding. Untr17 genomic regions were used as control sequences for negative PBX1 binding. The primers used for this assay were as follows: *Th distal site*, fwd gataaggcagcagcttccac, and rev cctctttcagcacggtgttt; *Th proximal site*, fwd gtctcctgtcccagaacacc and rev: aggcacctgcctctgaatc; Untr17 fwd ccaccacctgctgacacata and rev ttcaccttcattcgcttctg.

RNA isolation and qRT-PCR analysis

Eight-12-week-old male animals were used for RNA isolation and the qRT-PCR analysis. Total RNA from a single olfactory bulb was extracted using Trizol (Invitrogen) and 1 µg of RNA was reverse transcribed into cDNA using random primers and the SuperScript III First-Strand Synthesis System kit (Invitrogen). cDNA products were amplified using the Applied Biosystems QuantStudio5 Real-Time PCR System. All PCR reactions were performed using 10 µl of TaqMan Gene Expression Master Mix 2× (Applied Biosystems), 1 µl of TaqMan Gene Expression Assay 20×, 4 µl of cDNA (5 ng/µl) and water to reach a final volume of 20 µl/reaction. Specific TaqMan probes for mouse *Th* (Mm00447557 m1), *Slc6a3* (Mm00438388 m1), *Slc18a2* (Mm00553058 m1), *Gch1* (Mm01322973 m1), *Ddc* (Mm01192100 m1), *Meis2* (Mm00487748 m1) and *Gapdh* (Mm99999915 g1 as an endogenous control) were purchased from Applied Biosystems. Each sample was run in triplicate as a singleplex reaction system. In all experiments, samples containing no template were included as negative controls. The mRNA expression levels of the genes analyzed were represented as relative quantities (RQs) using the comparative threshold cycle method ($RQ=2^{-\Delta\Delta Ct}$) (Livak and Schmittgen, 2001). The threshold cycle values of each gene were normalized with respect to the housekeeping gene *Gapdh*.

Statistical analysis and graphical representation

All experiments were conducted blind to the genotype or experimental condition. All values are represented as the mean±s.e.m. For each experiment, the number of independent animals or cells is indicated as *n*. Applied statistical tests are indicated in the corresponding figure legends. Results were considered to be statistically significant when $*P<0.05$.

Acknowledgements

We thank Dr Licia Selleri for providing $Pbx1^{Fl/Fl}$ and *Pbx2* mutant animals and Pbx1 plasmids; Dr Oscar Marín and Dr Beatriz Rico labs for scientific discussion; Dr Pietro Fazzari for help with morphological reconstruction; Elia García for technical help; and Dr Oscar Marín, Dr Helena Mira and Dr Isabel Fariñas for comments on the manuscript.

Competing interests

The authors declare no competing or financial interests.

Author contributions

Conceptualization: N.F.; Methodology: L.R., I.R.-B., L.C., M.M., R.B.-R., A.P.-V., C.C., M.C., N.F.; Formal analysis: L.R., I.R.-B., L.C., M.M., R.B.-R., A.P.-V.; Investigation: L.R., I.R.-B.., L.C., M.M., R.B.-R., A.P.-V.; Data curation: N.F.; Writing - original draft: L.R., I.R.-B., L.C., M.M., R.B.-R., C.C., N.F.; Writing - review & editing: L.R., I.R.-B., L.C., M.M., R.B.-R., A.P.V., C.C., M.C., N.F.; Visualization: L.R., I.R.-B., L.C., M.M., N.F.; Supervision: N.F.; Project administration: N.F.; Funding acquisition: N.F.

Funding

This work was supported by PhD fellowships from the Ministerio de Educación, Cultura y Deporte (FPU16/02008 to I.R.-B.) and the Ministerio de Economía y Competitividad (BES-2012-053847 to L.R.. and BES-2015-072799 to R.B.-R.); by European Research Council grant (ERC-StG-2011-281920); by Ministerio de Economía y Competitividad grants (SAF2017-84790-R and SAF2016-75004R) and by the Generalitat Valenciana (PROMETEO/2018/055).

Supplementary information

Supplementary information available online at
http://dev.biologists.org/lookup/doi/10.1242/dev.186841.supplemental

Peer review history

The peer review history is available online at
https://dev.biologists.org/lookup/doi/10.1242/dev.186841.reviewer-comments.pdf

References

Agoston, Z., Heine, P., Brill, M. S., Grebbin, B. M., Hau, A.-C., Kallenborn-Gerhardt, W., Schramm, J., Götz, M. and Schulte, D. (2014). Meis2 is a Pax6 co-factor in neurogenesis and dopaminergic periglomerular fate specification in the adult olfactory bulb. *Development* **141**, 28-38. doi:10.1242/dev.097295

Arendt, D. (2008). The evolution of cell types in animals: emerging principles from molecular studies. *Nat. Rev. Genet.* **9**, 868-882. doi:10.1038/nrg2416

Arendt, D., Musser, J. M., Baker, C. V. H., Bergman, A., Cepko, C., Erwin, D. H., Pavlicev, M., Schlosser, G., Widder, S., Laubichler, M. D. et al. (2016). The origin and evolution of cell types. *Nat. Rev. Genet.* **17**, 744-757. doi:10.1038/nrg.2016.127

Arendt, D., Bertucci, P. Y., Achim, K. and Musser, J. M. (2019). Evolution of neuronal types and families. *Curr. Opin. Neurobiol.* **56**, 144-152. doi:10.1016/j.conb.2019.01.022

Bacon, C., Schneider, M., Le Magueresse, C., Froehlich, H., Sticht, C., Gluch, C., Monyer, H. and Rappold, G. A. (2015). Brain-specific Foxp1 deletion impairs neuronal development and causes autistic-like behaviour. *Mol. Psychiatry* **20**, 632-639. doi:10.1038/mp.2014.116

Banerjee, A., Marbach, F., Anselmi, F., Koh, M. S., Davis, M. B., Garcia da Silva, P., Delevich, K., Oyibo, H. K., Gupta, P., Li, B. et al. (2015). An interglomerular circuit gates glomerular output and implements gain control in the mouse olfactory bulb. *Neuron* **87**, 193-207. doi:10.1016/j.neuron.2015.06.019

Bohrer, C., Pfurr, S., Mammadzada, K., Schildge, S., Plappert, L., Hils, M., Pous, L., Rauch, K. S., Dumit, V. I., Pfeifer, D. et al. (2015). The balance of Id3 and E47 determines neural stem/precursor cell differentiation into astrocytes. *EMBO J.* **34**, 2804-2819. doi:10.15252/embj.201591118

Bonzano, S., Bovetti, S., Gendusa, C., Peretto, P. and De Marchis, S. (2016). Adult born olfactory bulb dopaminergic interneurons: molecular determinants and experience-dependent plasticity. *Front. Neurosci.* **10**, 7967. doi:10.3389/fnins.2016.00189

Borisovska, M., Bensen, A. L., Chong, G. and Westbrook, G. L. (2013). Distinct modes of dopamine and GABA release in a dual transmitter neuron. *J. Neurosci.* **33**, 1790-1796. doi:10.1523/JNEUROSCI.4342-12.2013

Boutin, C., Diestel, S., Desoeuvre, A., Tiveron, M.-C. and Cremer, H. (2008). Efficient in vivo electroporation of the postnatal rodent forebrain. *PLoS ONE* **3**, e1883. doi:10.1371/journal.pone.0001883

Bovetti, S., Bonzano, S., Garzotto, D., Giannelli, S. G., Iannielli, A., Armentano, M., Studer, M. and De Marchis, S. (2013). COUP-TFI controls activity-dependent tyrosine hydroxylase expression in adult dopaminergic olfactory bulb interneurons. *Development* **140**, 4850-4859. doi:10.1242/dev.089961

Brill, M. S., Snapyan, M., Wohlfrom, H., Ninkovic, J., Jawerka, M., Mastick, G. S., Ashery-Padan, R., Saghatelyan, A., Berninger, B. and Götz, M. (2008). A Dlx2- and Pax6-dependent transcriptional code for periglomerular neuron specification in the adult olfactory bulb. *J. Neurosci.* **28**, 6439-6452. doi:10.1523/JNEUROSCI.0700-08.2008

Capellini, T. D., Zewdu, R., Di Giacomo, G., Asciutti, S., Kugler, J. E., Di Gregorio, A. and Selleri, L. (2008). Pbx1/Pbx2 govern axial skeletal development by controlling Polycomb and Hox in mesoderm and Pax1/Pax9 in sclerotome. *Dev. Biol.* **321**, 500-514. doi:10.1016/j.ydbio.2008.04.005

Cave, J. W., Akiba, Y., Banerjee, K., Bhosle, S., Berlin, R. and Baker, H. (2010). Differential regulation of dopaminergic gene expression by Er81. *J. Neurosci.* **30**, 4717-4724. doi:10.1523/JNEUROSCI.0419-10.2010

Chen, C.-L., Broom, D. C., Liu, Y., De Nooij, J. C., Li, Z., Cen, C., Samad, O. A., Jessell, T. M., Woolf, C. J. and Ma, Q. (2006). Runx1 determines nociceptive sensory neuron phenotype and is required for thermal and neuropathic pain. *Neuron* **49**, 365-377. doi:10.1016/j.neuron.2005.10.036

Cubelos, B., Sebastián-Serrano, A., Kim, S., Moreno-Ortiz, C., Redondo, J. M., Walsh, C. A. and Nieto, M. (2008). Cux-2 controls the proliferation of neuronal intermediate precursors of the cortical subventricular zone. *Cereb. Cortex* **18**, 1758-1770. doi:10.1093/cercor/bhm199

Dardaei, L., Longobardi, E. and Blasi, F. (2014). Prep1 and Meis1 competition for Pbx1 binding regulates protein stability and tumorigenesis. *Proc. Natl. Acad. Sci. USA* **111**, E896-E905. doi:10.1073/pnas.1321200111

de Chevigny, A., Core, N., Follert, P., Wild, S., Bosio, A., Yoshikawa, K., Cremer, H. and Beclin, C. (2012). Dynamic expression of the pro-dopaminergic transcription factors Pax6 and Dlx2 during postnatal olfactory bulb neurogenesis. *Front. Cell Neurosci.* **6**, 6. doi:10.3389/fncel.2012.00006

Delile, J., Rayon, T., Melchionda, M., Edwards, A., Briscoe, J. and Sagner, A. (2019). Single cell transcriptomics reveals spatial and temporal dynamics of gene expression in the developing mouse spinal cord. *Development* **146**, dev173807. doi:10.1242/dev.173807

Deneris, E. S. and Hobert, O. (2014). Maintenance of postmitotic neuronal cell identity. *Nat. Neurosci.* **17**, 899-907. doi:10.1038/nn.3731

Denes, A. S., Jékely, G., Steinmetz, P. R. H., Raible, F., Snyman, H., Prud'homme, B., Ferrier, D. E. K., Balavoine, G. and Arendt, D. (2007). Molecular architecture of annelid nerve cord supports common origin of nervous system centralization in bilateria. *Cell* **129**, 277-288. doi:10.1016/j.cell.2007.02.040

Doitsidou, M., Flames, N., Topalidou, I., Abe, N., Felton, T., Remesal, L., Popovitchenko, T., Mann, R., Chalfie, M. and Hobert, O. (2013). A combinatorial regulatory signature controls terminal differentiation of the dopaminergic nervous system in C. elegans. *Genes Dev.* **27**, 1391-1405. doi:10.1101/gad.217224.113

Donovan, L. J., Spencer, W. C., Kitt, M. M., Eastman, B. A., Lobur, K. J., Jiao, K., Silver, J. and Deneris, E. S. (2019). Lmx1b is required at multiple stages to build expansive serotonergic axon architectures. *eLife* **8**, e48788. doi:10.7554/elife.48788

Erbel-Sieler, C., Dudley, C., Zhou, Y., Wu, X., Estill, S. J., Han, T., Diaz-Arrastia, R., Brunskill, E. W., Potter, S. S. and McKnight, S. L. (2004). Behavioral and regulatory abnormalities in mice deficient in the NPAS1 and NPAS3 transcription factors. *Proc. Natl. Acad. Sci. USA* **101**, 13648-13653. doi:10.1073/pnas.0405310101

Feng, W., Li, Y., Dao, P., Aburas, J., Islam, P., Elbaz, B., Kolarzyk, A., Brown, A. E. X. and Kratsios, P. (2020). A terminal selector prevents a Hox transcriptional switch to safeguard motor neuron identity throughout life. *eLife* **9**, e50065. doi:10.7554/eLife.50065

Fernández, M. E., Croce, S., Boutin, C., Cremer, H. and Raineteau, O. (2011). Targeted electroporation of defined lateral ventricular walls: a novel and rapid method to study fate specification during postnatal forebrain neurogenesis. *Neural Dev.* **6**, 13. doi:10.1186/1749-8104-6-13

Ferretti, E., Li, B., Zewdu, R., Wells, V., Hebert, J. M., Karner, C., Anderson, M. J., Williams, T., Dixon, J., Dixon, M. J. et al. (2011). A conserved Pbx-Wnt-p63-Irf6 regulatory module controls face morphogenesis by promoting epithelial apoptosis. *Dev. Cell* **21**, 627-641. doi:10.1016/j.devcel.2011.08.005

Flames, N. and Hobert, O. (2009). Gene regulatory logic of dopamine neuron differentiation. *Nature* **458**, 885-889. doi:10.1038/nature07929

Flames, N. and Hobert, O. (2011). Transcriptional control of the terminal fate of monoaminergic neurons. *Annu. Rev. Neurosci.* **34**, 153-184. doi:10.1146/annurev-neuro-061010-113824

Furlanis, E. and Scheiffele, P. (2018). Regulation of neuronal differentiation, function, and plasticity by alternative splicing. *Annu. Rev. Cell Dev. Biol.* **34**, 451-469. doi:10.1146/annurev-cellbio-100617-062826

Gaborieau, E., Hurtado-Chong, A., Fernández, M., Azim, K. and Raineteau, O. (2018). A dual role for the transcription factor Sp8 in postnatal neurogenesis. *Sci. Rep.* **8**, 14560. doi:10.1038/s41598-018-32134-6

Gabut, M., Samavarchi-Tehrani, P., Wang, X., Slobodeniuc, V., O'Hanlon, D., Sung, H.-K., Alvarez, M., Talukder, S., Pan, Q., Mazzoni, E. O. et al. (2011). An alternative splicing switch regulates embryonic stem cell pluripotency and reprogramming. *Cell* **147**, 132-146. doi:10.1016/j.cell.2011.08.023

Galliano, E., Franzoni, E., Breton, M., Chand, A. N., Byrne, D. J., Murthy, V. N. and Grubb, M. S. (2018). Embryonic and postnatal neurogenesis produce functionally distinct subclasses of dopaminergic neuron. *eLife* **7**, e32373. doi:10.7554/eLife.32373

Garcia-Cuellar, M.-P., Steger, J., Füller, E., Hetzner, K. and Slany, R. K. (2015). Pbx3 and Meis1 cooperate through multiple mechanisms to support Hox-induced murine leukemia. *Haematologica* **100**, 905-913. doi:10.3324/haematol.2015.124032

Grebbin, B. M., Hau, A.-C., Groß, A., Anders-Maurer, M., Schramm, J., Koss, M., Wille, C., Mittelbronn, M., Selleri, L. and Schulte, D. (2016). PBX1 is required for adult subventricular zone neurogenesis. *Development* **143**, 2281-2291. doi:10.1242/dev.128033

Guo, C., Eckler, M. J., McKenna, W. L., McKinsey, G. L., Rubenstein, J. L. R. and Chen, B. (2013). Fezf2 expression identifies a multipotent progenitor for neocortical projection neurons, astrocytes, and oligodendrocytes. *Neuron* **80**, 1167-1174. doi:10.1016/j.neuron.2013.09.037

Hack, M. A., Saghatelyan, A., De Chevigny, A., Pfeifer, A., Ashery-Padan, R., Lledo, P.-M. and Götz, M. (2005). Neuronal fate determinants of adult olfactory bulb neurogenesis. *Nat. Neurosci.* **8**, 865-872. doi:10.1038/nn1479

Hobert, O. (2008). Regulatory logic of neuronal diversity: terminal selector genes and selector motifs. *Proc. Natl. Acad. Sci. USA* **105**, 20067-20071. doi:10.1073/pnas.0806070105

Hobert, O. (2011). Regulation of terminal differentiation programs in the nervous system. *Annu. Rev. Cell Dev. Biol.* **27**, 681-696. doi:10.1146/annurev-cellbio-092910-154226

Hobert, O. and Kratsios, P. (2019). Neuronal identity control by terminal selectors in worms, flies, and chordates. *Curr. Opin. Neurobiol.* **56**, 97-105. doi:10.1016/j.conb.2018.12.006

Huynh, M. A., Ikeuchi, Y., Netherton, S., de la Torre-Ubieta, L., Kanadia, R., Stegmüller, J., Cepko, C., Bonni, S. and Bonni, A. (2011). An isoform-specific SnoN1-FOXO1 repressor complex controls neuronal morphogenesis and positioning in the mammalian brain. *Neuron* **69**, 930-944. doi:10.1016/j.neuron.2011.02.008

Iulianella, A., Sharma, M., Durnin, M., Vanden Heuvel, G. B. and Trainor, P. A. (2008). Cux2 (Cutl2) integrates neural progenitor development with cell-cycle progression during spinal cord neurogenesis. *Development* **135**, 729-741. doi:10.1242/dev.013276

Kiyokage, E., Pan, Y.-Z., Shao, Z., Kobayashi, K., Szabo, G., Yanagawa, Y., Obata, K., Okano, H., Toida, K., Puche, A. C. et al. (2010). Molecular identity of periglomerular and short axon cells. *J. Neurosci.* **30**, 1185-1196. doi:10.1523/JNEUROSCI.3497-09.2010

Kohwi, M., Petryniak, M. A., Long, J. E., Ekker, M., Obata, K., Yanagawa, Y., Rubenstein, J. L. R. and Alvarez-Buylla, A. (2007). A subpopulation of olfactory bulb GABAergic interneurons is derived from Emx1- and Dlx5/6-expressing progenitors. *J. Neurosci.* **27**, 6878-6891. doi:10.1523/JNEUROSCI.0254-07.2007

Kosaka, T. and Kosaka, K. (2016). Neuronal organization of the main olfactory bulb revisited. *Anat. Sci. Int.* **91**, 115-127. doi:10.1007/s12565-015-0309-7

Koss, M., Bolze, A., Brendolan, A., Saggese, M., Capellini, T. D., Bojilova, E., Boisson, B., Prall, O. W. J., Elliott, D. A., Solloway, M. et al. (2012). Congenital asplenia in mice and humans with mutations in a Pbx/Nkx2-5/p15 module. *Dev. Cell* **22**, 913-926. doi:10.1016/j.devcel.2012.02.009

Linares, A. J., Lin, C.-H., Damianov, A., Adams, K. L., Novitch, B. G. and Black, D. L. (2015). The splicing regulator PTBP1 controls the activity of the transcription factor Pbx1 during neuronal differentiation. *eLife* **4**, e09268. doi:10.7554/eLife.09268

Lindeberg, J., Usoskin, D., Bengtsson, H., Gustafsson, A., Kylberg, A., Söderström, S. and Ebendal, T. (2004). Transgenic expression of Cre recombinase from the tyrosine hydroxylase locus. *Genesis* **40**, 67-73. doi:10.1002/gene.20065

Liu, C., Maejima, T., Wyler, S. C., Casadesus, G., Herlitze, S. and Deneris, E. S. (2010). Pet-1 is required across different stages of life to regulate serotonergic function. *Nat. Neurosci.* **13**, 1190-1198. doi:10.1038/nn.2623

Livak, K. J. and Schmittgen, T. D. (2001). Analysis of relative gene expression data using real-time quantitative PCR and the $2^{-\Delta\Delta CT}$ method. *Methods* **25**, 402-408. doi:10.1006/meth.2001.1262

Lloret-Fernández, C., Maicas, M., Mora-Martínez, C., Artacho, A., Jimeno-Martín, Á., Chirivella, L., Weinberg, P. and Flames, N. (2018). A transcription factor collective defines the HSN serotonergic neuron regulatory landscape. *eLife* **7**, e32785. doi:10.7554/eLife.32785

Lodato, S., Molyneaux, B. J., Zuccaro, E., Goff, L. A., Chen, H.-H., Yuan, W., Meleski, A., Takahashi, E., Mahony, S., Rinn, J. L. et al. (2014). Gene co-regulation by Fezf2 selects neurotransmitter identity and connectivity of corticospinal neurons. *Nat. Neurosci.* **17**, 1046-1054. doi:10.1038/nn.3757

Longobardi, E., Penkov, D., Mateos, D., De Florian, G., Torres, M. and Blasi, F. (2014). Biochemistry of the tale transcription factors PREP, MEIS, and PBX in vertebrates. *Dev. Dyn.* **243**, 59-75. doi:10.1002/dvdy.24016

Luria, V., Krawchuk, D., Jessell, T. M., Laufer, E. and Kania, A. (2008). Specification of motor axon trajectory by Ephrin-B:EphB signaling: symmetrical control of axonal patterning in the developing limb. *Neuron* **60**, 1039-1053. doi:10.1016/j.neuron.2008.11.011

Magno, L., Kretz, O., Bert, B., Ersözlü, S., Vogt, J., Fink, H., Kimura, S., Vogt, A., Monyer, H., Nitsch, R. et al. (2011). The integrity of cholinergic basal forebrain neurons depends on expression of Nkx2-1. *Eur. J. Neurosci.* **34**, 1767-1782. doi:10.1111/j.1460-9568.2011.07890.x

Mayer, C., Hafemeister, C., Bandler, R. C., Machold, R., Batista Brito, R., Jaglin, X., Allaway, K., Butler, A., Fishell, G. and Satija, R. (2018). Developmental diversification of cortical inhibitory interneurons. *Nature* **555**, 457-462. doi:10.1038/nature25999

McEvilly, R. J., Ortiz de Diaz, M., Schonemann, M. D., Hooshmand, F. and Rosenfeld, M. G. (2002). Transcriptional regulation of cortical neuron migration by POU domain factors. *Science* **295**, 1528-1532. doi:10.1126/science.1067132

Merkle, F. T., Mirzadeh, Z. and Alvarez-Buylla, A. (2007). Mosaic organization of neural stem cells in the adult brain. *Science* **317**, 381-384. doi:10.1126/science.1144914

Mi, D., Li, Z., Lim, L., Li, M., Moissidis, M., Yang, Y., Gao, T., Hu, T. X., Pratt, T., Price, D. J. et al. (2018). Early emergence of cortical interneuron diversity in the mouse embryo. *Science* **360**, 81-85. doi:10.1126/science.aar6821

Nóbrega-Pereira, S., Kessaris, N., Du, T., Kimura, S., Anderson, S. A. and Marín, O. (2008). Postmitotic Nkx2-1 controls the migration of telencephalic interneurons by direct repression of guidance receptors. *Neuron* **59**, 733-745. doi:10.1016/j.neuron.2008.07.024

Nomaksteinsky, M., Kassabov, S., Chettouh, Z., Stoeklé, H.-C., Bonnaud, L., Fortin, G., Kandel, E. R. and Brunet, J.-F. (2013). Ancient origin of somatic and visceral neurons. *BMC Biol.* **11**, 53. doi:10.1186/1741-7007-11-53

Nowakowski, T. J., Bhaduri, A., Pollen, A. A., Alvarado, B., Mostajo-Radji, M. A., Di Lullo, E., Haeussler, M., Sandoval-Espinosa, C., Liu, S. J., Velmeshev, D. et al. (2017). Spatiotemporal gene expression trajectories reveal developmental hierarchies of the human cortex. *Science* **358**, 1318-1323. doi:10.1126/science.aap8809

Patel, T. and Hobert, O. (2017). Coordinated control of terminal differentiation and restriction of cellular plasticity. *eLife* **6**, e24100. doi:10.7554/eLife.24100.001

Penkov, D., San Martín, D. M., Fernandez-Díaz, L. C., Rosselló, C. A., Torroja, C., Sánchez-Cabo, F., Warnatz, H. J., Sultan, M., Yaspo, M. L., Gabrieli, A. et al. (2013). Analysis of the DNA-binding profile and function of TALE homeoproteins reveals their specialization and specific interactions with Hox genes/proteins. *Cell Rep.* **3**, 1321-1333. doi:10.1016/j.celrep.2013.03.029

Perez-Villalba, A., Sirerol-Piquer, M. S., Belenguer, G., Soriano-Cantón, R., Muñoz-Manchado, A. B., Villadiego, J., Alarcón-Arís, D., Soria, F. N., Dehay, B., Bezard, E. et al. (2018). Synaptic regulator α-synuclein in dopaminergic fibers is essentially required for the maintenance of subependymal neural stem cells. *J. Neurosci.* **38**, 814-825. doi:10.1523/JNEUROSCI.2276-17.2017

Pfurr, S., Chu, Y.-H., Bohrer, C., Greulich, F., Beattie, R., Mammadzada, K., Hils, M., Arnold, S. J., Taylor, V., Schachtrup, K. et al. (2017). The E2A splice variant E47 regulates the differentiation of projection neurons via p57(KIP2) during cortical development. *Development* **144**, 3917-3931. doi:10.1242/dev.145698

Pignatelli, A. and Belluzzi, O. (2017). Dopaminergic neurones in the main olfactory bulb: an overview from an electrophysiological perspective. *Front. Neuroanat.* **11**, 7. doi:10.3389/fnana.2017.00007

Porter, R. S., Jaamour, F. and Iwase, S. (2018). Neuron-specific alternative splicing of transcriptional machineries: implications for neurodevelopmental disorders. *Mol. Cell. Neurosci.* **87**, 35-45. doi:10.1016/j.mcn.2017.10.006

Qiu, M., Bulfone, A., Martinez, S., Meneses, J. J., Shimamura, K., Pedersen, R. A. and Rubenstein, J. L. R. (1995). Null mutation of Dlx-2 results in abnormal morphogenesis of proximal first and second branchial arch derivatives and abnormal differentiation in the forebrain. *Genes Dev.* **9**, 2523-2538. doi:10.1101/gad.9.20.2523

Raj, B., O'Hanlon, D., Vessey, J. P., Pan, Q., Ray, D., Buckley, N. J., Miller, F. D. and Blencowe, B. J. (2011). Cross-regulation between an alternative splicing activator and a transcription repressor controls neurogenesis. *Mol. Cell* **43**, 843-850. doi:10.1016/j.molcel.2011.08.014

Reiter, F., Wienerroither, S. and Stark, A. (2017). Combinatorial function of transcription factors and cofactors. *Curr. Opin. Genet. Dev.* **43**, 73-81. doi:10.1016/j.gde.2016.12.007

Rhee, H. S., Closser, M., Guo, Y., Bashkirova, E. V., Tan, G. C., Gifford, D. K. and Wichterle, H. (2016). Expression of terminal effector genes in mammalian neurons is maintained by a dynamic relay of transient enhancers. *Neuron* **92**, 1252-1265. doi:10.1016/j.neuron.2016.11.037

Rubenstein, J. L. R. and Rakic, P. (2013). Patterning and cell type specification in the developing CNS and PNS. In *Comprehensive Developmental Neuroscience* (ed. J. L. R. Rubenstein and P. Rakic), Chapter 1, pp. 3-24. Elsevier. doi:10.1016/c2011-0-07685-8

Saino-Saito, S., Sasaki, H., Volpe, B. T., Kobayashi, K., Berlin, R. and Baker, H. (2004). Differentiation of the dopaminergic phenotype in the olfactory system of neonatal and adult mice. *J. Comp. Neurol.* **479**, 389-398. doi:10.1002/cne.20320

Selleri, L., DiMartino, J., van Deursen, J., Brendolan, A., Sanyal, M., Boon, E., Capellini, T., Smith, K. S., Rhee, J., Popperl, H. et al. (2004). The TALE homeodomain protein Pbx2 is not essential for development and long-term survival. *Mol. Cell. Biol.* **24**, 5324-5331. doi:10.1128/mcb.24.12.5324-5331.2004

Sgadò, P., Ferretti, E., Grbec, D., Bozzi, Y. and Simon, H. H. (2012). The atypical homeoprotein Pbx1a participates in the axonal pathfinding of mesencephalic dopaminergic neurons. *Neural Dev.* **7**, 24. doi:10.1186/1749-8104-7-24

Shirasaki, R., Lewcock, J. W., Lettieri, K. and Pfaff, S. L. (2006). FGF as a target-derived chemoattractant for developing motor axons genetically programmed by the LIM code. *Neuron* **50**, 841-853. doi:10.1016/j.neuron.2006.04.030

Sousa, V. H., Miyoshi, G., Hjerling-Leffler, J., Karayannis, T. and Fishell, G. (2009). Characterization of Nkx6-2-derived neocortical interneuron lineages. *Cereb. Cortex* **19**, i1-i10. doi:10.1093/cercor/bhp038

Sugitani, Y., Nakai, S., Minowa, O., Nishi, M., Jishage, K. I., Kawano, H., Mori, K., Ogawa, M. and Noda, T. (2002). Brn-1 and Brn-2 share crucial roles in the production and positioning of mouse neocortical neurons. *Genes Dev.* **16**, 1760-1765. doi:10.1101/gad.978002

Sussel, L., Marin, O., Kimura, S. and Rubenstein, J. L. R. (1999). Loss of Nkx2.1 homeobox gene function results in a ventral to dorsal molecular respecification within the basal telencephalon: evidence for a transformation of the pallidum into the striatum. *Development* **126**, 3359-3370.

Tapial, J., Ha, K. C. H., Sterne-Weiler, T., Gohr, A., Braunschweig, U., Hermoso-Pulido, A., Quesnel-Vallières, M., Permanyer, J., Sodaei, R., Marquez, Y. et al. (2017). An atlas of alternative splicing profiles and functional associations reveals new regulatory programs and genes that simultaneously express multiple major isoforms. *Genome Res.* **27**, 1759-1768. doi:10.1101/gr.220962.117

Tiveron, M.-C., Beclin, C., Murgan, S., Wild, S., Angelova, A., Marc, J., Coré, N., de Chevigny, A., Herrera, E., Bosio, A. et al. (2017). Zic-proteins are repressors of dopaminergic forebrain fate in mice and C. Elegans. *J. Neurosci.* **37**, 10611-10623. doi:10.1523/JNEUROSCI.3888-16.2017

Tomer, R., Denes, A. S., Tessmar-Raible, K. and Arendt, D. (2010). Profiling by image registration reveals common origin of annelid mushroom bodies and vertebrate pallium. *Cell* **142**, 800-809. doi:10.1016/j.cell.2010.07.043

Vergaño-Vera, E., Yusta-Boyo, M. J., de Castro, F., Bernad, A., de Pablo, F. and Vicario-Abejón, C. (2006). Generation of GABAergic and dopaminergic interneurons from endogenous embryonic olfactory bulb precursor cells. *Development* **133**, 4367-4379. doi:10.1242/dev.02601

Villaescusa, J. C., Li, B., Toledo, E. M., Rivetti di Val Cervo, P., Yang, S., Stott, S. R. W., Kaiser, K., Islam, S., Gyllborg, D., Laguna-Goya, R. et al. (2016). A PBX1 transcriptional network controls dopaminergic neuron development and is impaired in Parkinson's disease. *EMBO J.* **35**, 1963-1978. doi:10.15252/embj.201593725

Vuong, C. K., Black, D. L. and Zheng, S. (2016). The neurogenetics of alternative splicing. *Nat. Rev. Neurosci.* **17**, 265-281. doi:10.1038/nrn.2016.27

Weihe, E., Depboylu, C., Schütz, B., Schäfer, M. K.-H. and Eiden, L. E. (2006). Three types of tyrosine hydroxylase-positive CNS neurons distinguished by dopa decarboxylase and VMAT2 co-expression. *Cell. Mol. Neurobiol.* **26**, 657-676. doi:10.1007/s10571-006-9053-9

Zhou, X., Liu, F., Tian, M., Xu, Z., Liang, Q., Wang, C., Li, J., Liu, Z., Tang, K., He, M. et al. (2015). Transcription factors COUP-TFI and COUP-TFII are required for the production of granule cells in the mouse olfactory bulb. *Development* **142**, 1593-1605. doi:10.1242/dev.115279

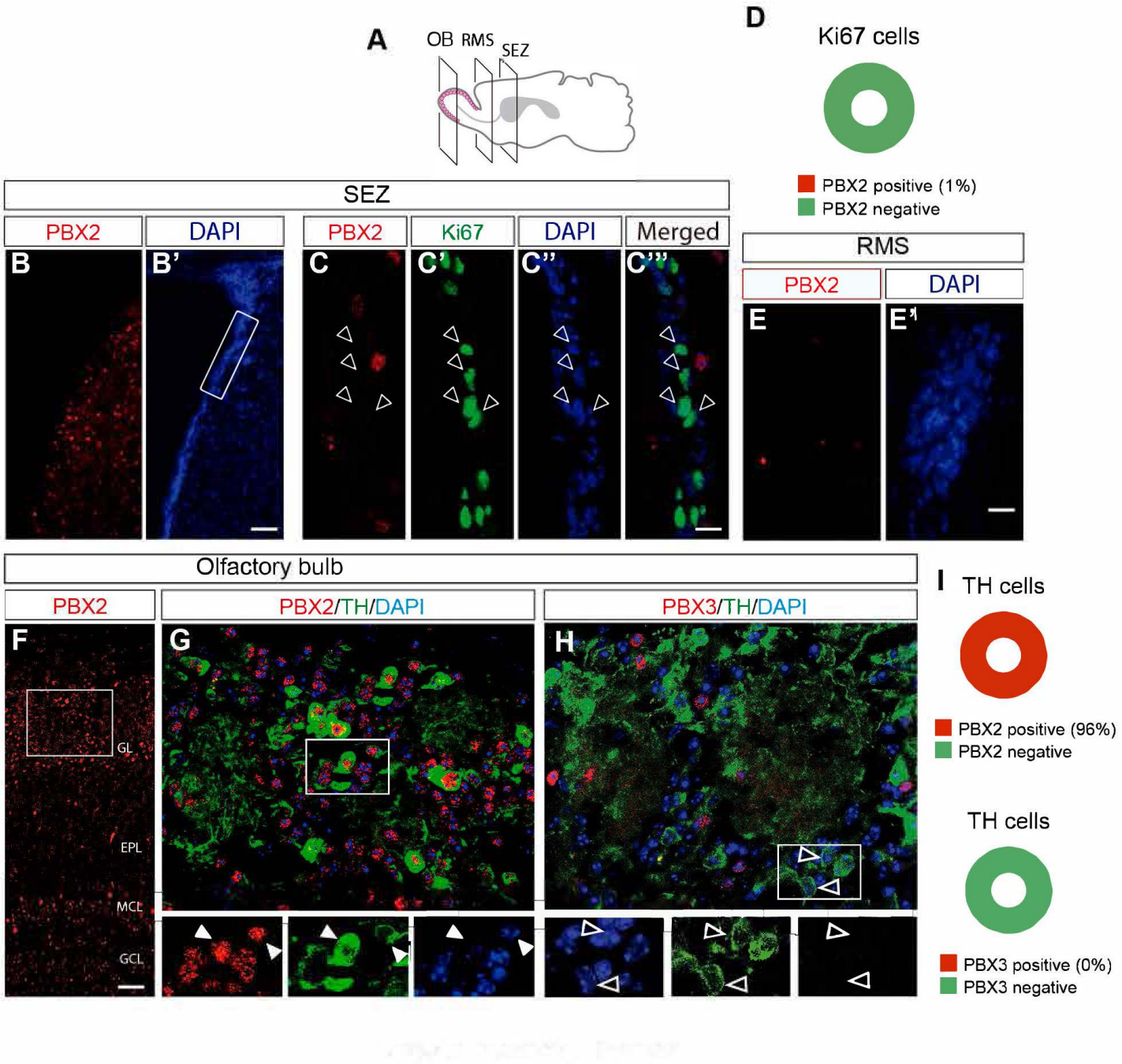

Fig. S1. PBX2 expression analysis in olfactory bulb adult neurogenesis.
A) Brain representation of the coronal levels analyzed in the micrographs. OB: olfactory bulb, RMS: rostral migratory stream, SEZ: subependymal zone. B) PBX2 expression in the SEZ region. Scale bar: 50 μm. C) Analysis of PBX2 expression in proliferating progenitors by double PBX2 and Ki67 immunostaining. Scale bar: 10 μm. D) Quantification of PBX2 expression in proliferating progenitors. E) Analysis of PBX2 expression in RMS shows no-expression in migrating neuroblasts. Scale bar: 20 μm. F) PBX2 expression in the OB. EPL: external plexiform layer, GCL: granular cell layer, GL: glomerular layer, MCL: mitral cell layer. Scale bar: 75 μm. G) Double immunostaining of TH and PBX2 in the OB. H) Double immunostaining of TH and PBX3 in the OB. Scale bar: 20 μm. I)Quantification of PBX2 and PBX3 expression in TH-positive cells.

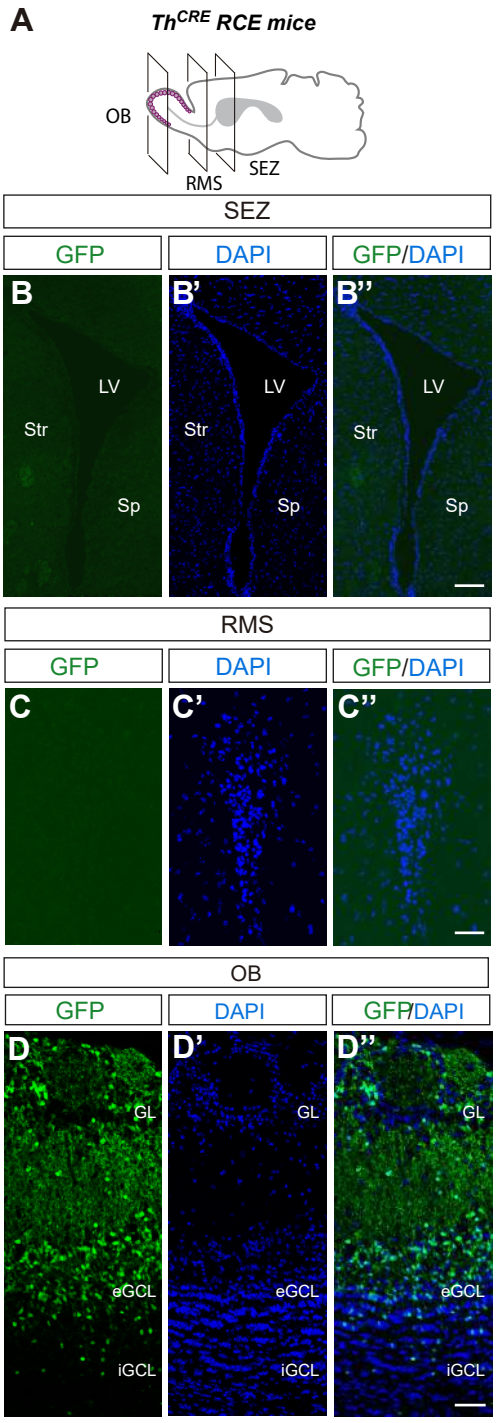

Supplementary Figure 2

Figure S2. *Th*^{CRE} lineage tracing in olfactory bulb adult neurogenesis.
A) Brain representation of the coronal levels analyzed in the micrographs. OB: olfactory bulb, RMS: rostral migratory stream, SEZ: subependymal zone. **B**) *Th*^{CRE}, RCE animals do not show GFP expression in adult SEZ. Scale bar: 50 μm. **C**) *Th*^{CRE}, RCE animals do not show GFP expression in adult RMS. Scale bar: 40 μm. **D**) *Th*^{CRE}, RCE animals show GFP expression in the external granular cell layer and the glomerular layer of the adult olfactory bulb. Scale bar: 75 μm.

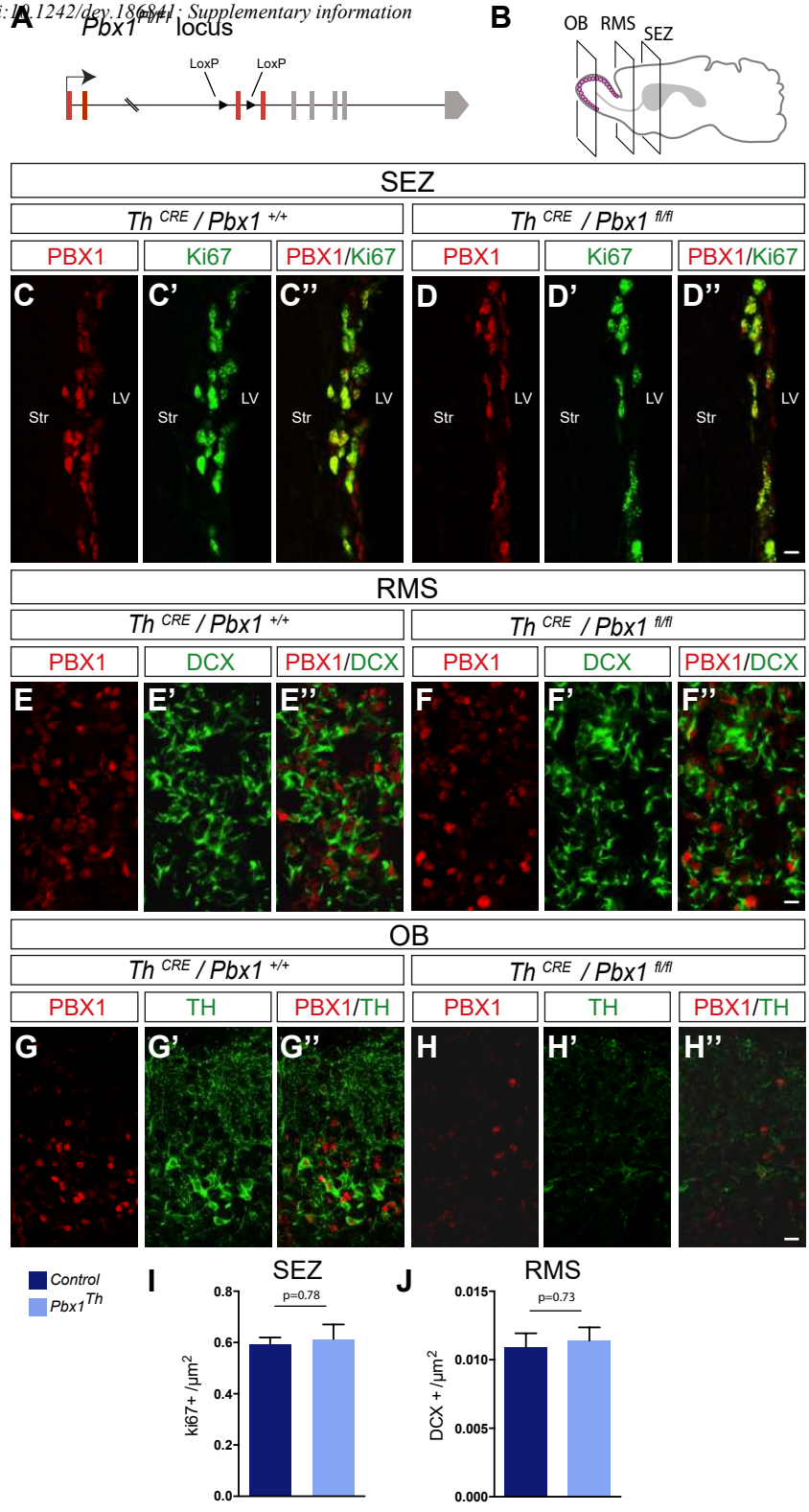

Supplementary Figure 3

Figure S3. *Pbx1*Th mutants specifically remove *Pbx1* from differentiating DA neurons in the OB. A) *Pbx1* locus in Pbx1$^{fl/fl}$ animals contains LoxP sites flanking the third exon. Red boxes indicate the exons coding for the DNA binding domain. **B**) Brain representation of the coronal levels analyzed in the micrographs. OB: olfactory bulb, RMS: rostral migratory stream, SEZ: subependymal zone. **C**) PBX1 expression in SEZ proliferating progenitors (Ki67 positive) in *Th*^{CRE}, RCE, Pbx1$^{+/+}$ animals. **D**) PBX1 expression in SEZ proliferating progenitors (Ki67 positive) in *Th*^{CRE}, RCE, Pbx1$^{fl/fl}$ mutants. **E**) PBX1 expression in RMS migrating neuroblasts (DCX positive) of *Th*^{CRE}, RCE, Pbx1$^{+/+}$ animals. **F**) PBX1 expression in RMS migrating neuroblasts (DCX positive) of *Th*^{CRE}, RCE, Pbx1$^{fl/fl}$ mutants. **G**) PBX1 expression in OB DA lineage labeled by GFP and TH expression in *Th*^{CRE}, RCE, Pbx1$^{+/+}$ animals. **H**) PBX1 expression is reduced in OB of *Th*^{CRE}, RCE, Pbx1$^{fl/fl}$ animals. **I**) Quantification of proliferating progenitors (Ki67 positive) in controls and *Pbx1*Th mutants. n=3 animals each genotype. Student's t test. **J**)Quantification of RMS migrating neuroblasts (DCX positive) in controls and *Pbx1*Th mutants. n=3 animals. each genotype. Student's t test. Scale bars: 10 µm.

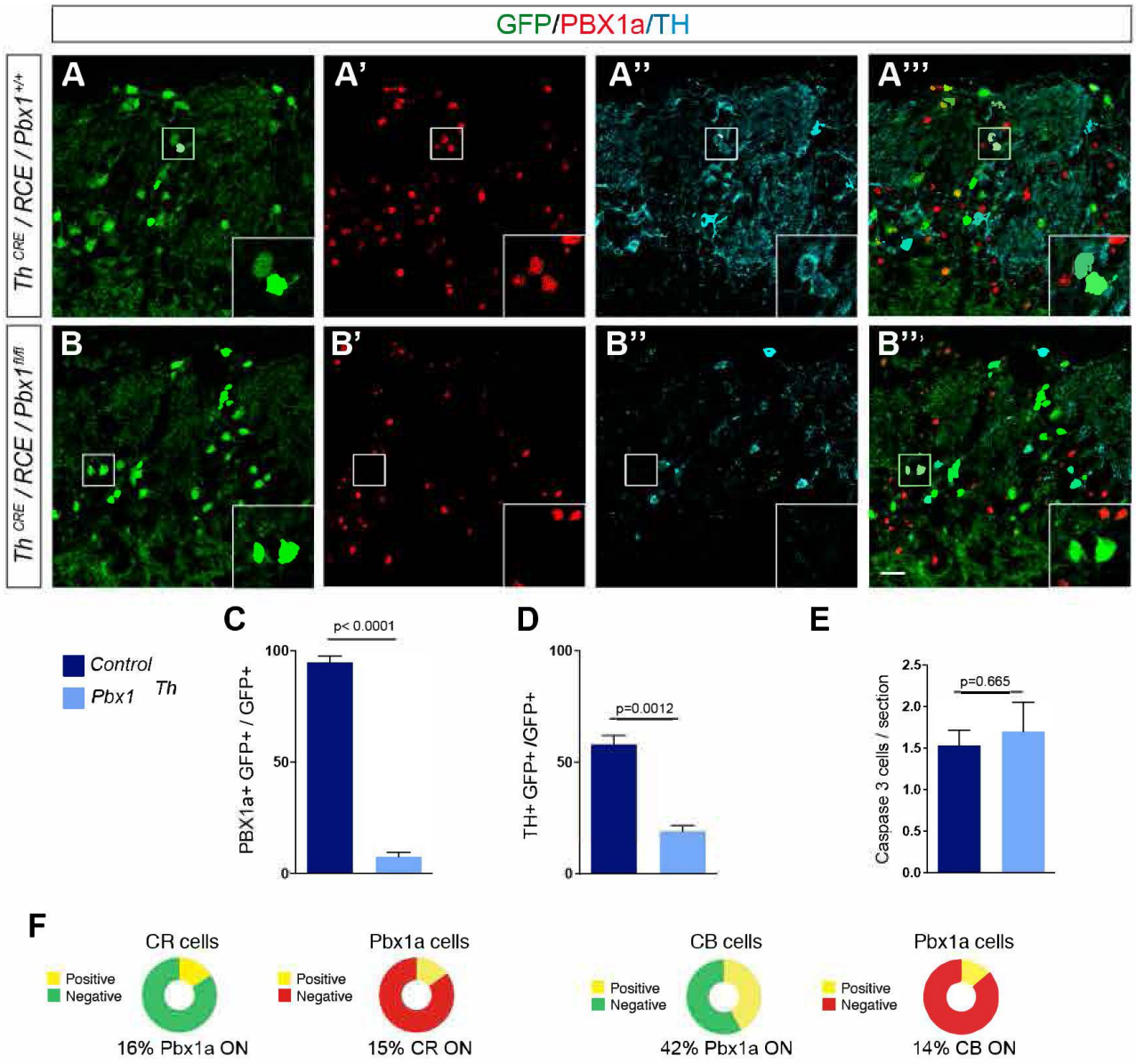

Figure S4. *Pbx1*Th mutants efficiently remove Pbx1 from DA lineage cells in OB.
A) GFP, PBX1a and TH co-expression in *Th*^{CRE}, *RCE*, *Pbx1*$^{+/+}$ animals. B) GFP, PBX1a and TH co-expression in *Th*^{CRE}, *RCE*, *Pbx1*$^{fl/fl}$ animals show both PBX1 a and TH expression defects in the DA lineage. Scale bar: 25 µm. C) Percentage of GFP positive cells co-expressing PBX1A in controls and *Pbx1*Th mutants. n=3 animals each genotype, Student's t test, unpaired, two tail. D) Percentage of GFP/RCE positive cells co-expressing TH in controls and *Pbx1*Th mutants. n=3 animals each genotype, Student's t test, unpaired, two tail. E) Cell death quantification with Caspase 3 antibody in controls and *Pbx1*Th mutants. n=3 animals each genotype, Student's t test, unpaired, two tail. F) Quantification of double CR/PBX1a and CB/PBX1a positive cells in OB of control animals. n=3 animals each genotype.

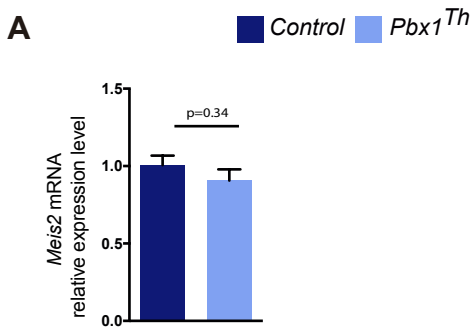

Supplementary Figure 5

Figure S5. *Meis2* transcription is unaffected in *Pbx1Th* mutants. A) *Meis2* mRNA expression level in controls and *Pbx1Th* mutants measured by quantitative RT-PCR. Controls n=4 animals, *Pbx1Th* n=3 animals, Student´s t test.

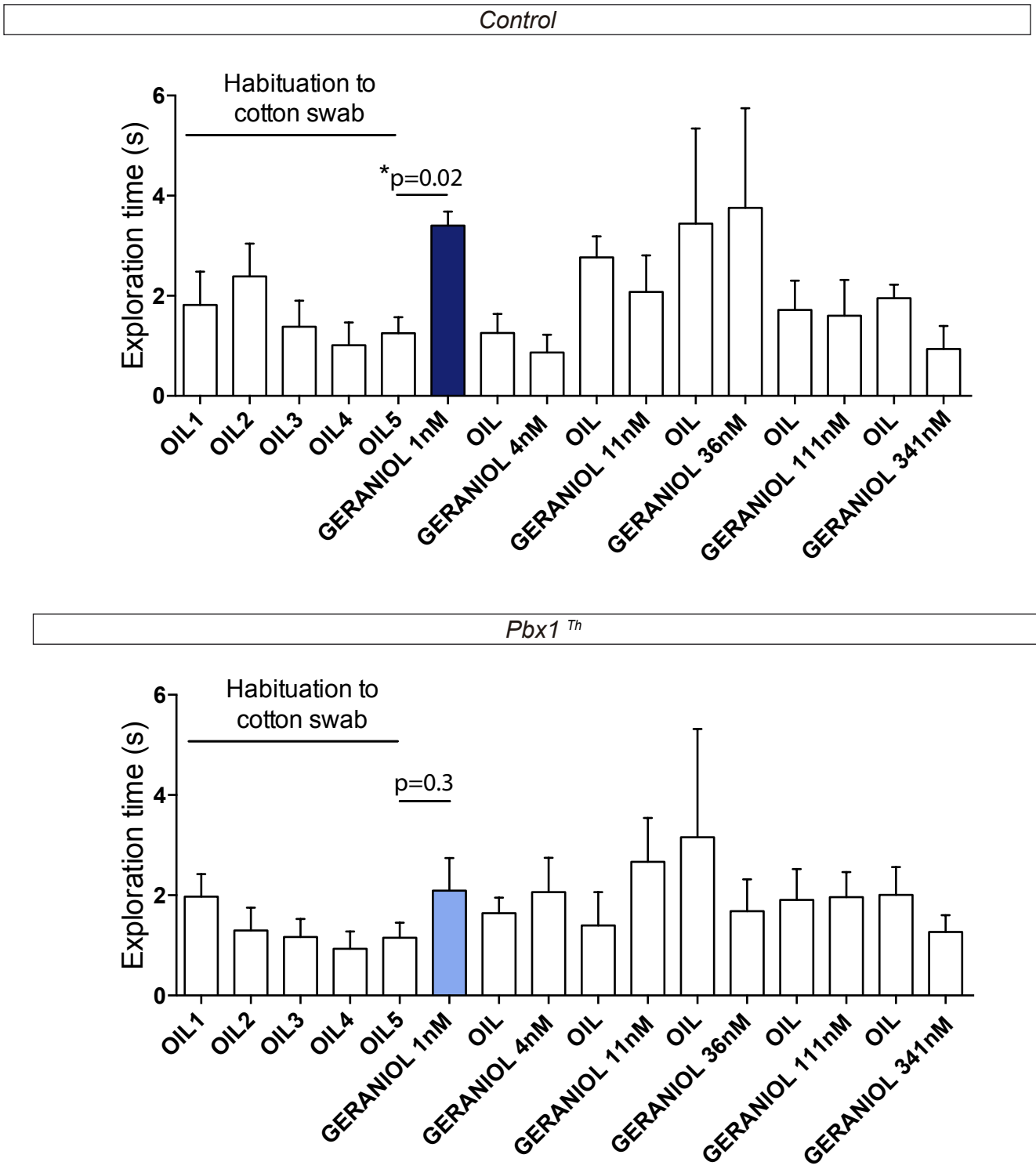

Supplementary Figure 6

Figure S6. *Pbx1Th* mutants show odor detection threshold deficits. In the odor threshold paradigm, mice are first habituated to the presence of the cotton swab without odorant (OIL1 to OIL5) and then their reaction to increasing concentrations of geraniol is analyzed. Control mice detect Geraniol at 1 nM while *Pbx1Th* mutants do not significantly react to this concentration. *Pbx1Th* mutants show high variability in their response compared to the control group precluding the establishment of a specific threshold value. n=5 control animals, n=8 *Pbx1Th* mutant animals. Paired Student´s t test.

Table S1. Quantification primary data.

Figure 1E	*TH+ cells/mm2:* control 418±16, *Pbx2*$^{-/-}$ 441±12, *Pbx1*Th mice 178±6, *Pbx1*Th *and Pbx2*$^{-/-}$ 131±7. n=3 animals each genotype.
Figure 1I	*GFP+ cells/mm*^{2}: control 616±17, *Pbx1*Th 628±48. n=3 animals each genotype.
Figure 1L	*TH+ cells/mm*^{2}: control 172±8, *Pbx1*Th 109±7. n=3 animals each genotype.
Figure 1N	*PGL BrdU+ cells/section*: control 11±2, *Pbx1*Th 16±3. n=3 animals each genotype.
Figure 1O	*TH+/BrdU+ cells*: control 19±2%, *Pbx1*Th 8±2%. n=3 animals each genotype.
Figure 1P	*CR+/BrdU+ cells*: control 21±3%, *Pbx1*Th 19±2%. n=3 animals each genotype.
Figure 1Q	*CB+/BrdU+ cells*: control 5±1%, *Pbx1*Th 4±2%. n=3 animals each genotype.
Figure 2C	*COUPTF1+ GFP+/GFP+:* control 56±4%, *Pbx1*Th 53±2%. n=3 animals each genotype.
Figure 2F	*ETV1+ GFP+/GFP+*: control 62±6%, *Pbx1*Th 60±1%. n=3 animals each genotype.
Figure 2I	*PAX6+ GFP+/GFP+:* control 83±2%, *Pbx1*Th 77±1%. n=3 animals each genotype.
Figure 2L	*DLX+ GFP+/GFP+:* control 93±0.4%, *Pbx1*Th 96±0.05%. n=3 animals each genotype.
Figure 2O	*MEIS2+ GFP+/GFP+:* control 84±1%, *Pbx1*Th 39±1%. n=3 animals each genotype.
Figure 3D	*Relative expression levels*: control *Ddc* 1±0.2, *Vmat2* 1±0.1, *Dat* 1±0.1, *Gch* 1±0.1, n=4 animals; *Pbx1*Th *Ddc* 0.5±0.05, *Vmat2* 0.4±0.1, *Dat* 0.5±0.1, *Gch* 1±0.1, n=3 animals.
Figure 4D	*GFP+ pixels/pixels*: control 10±1.4%, *Pbx1*Th 5±0.5%. n=3 animals each genotype. *Glomerulus area (μm*^{2}): control 6050±267, *Pbx1*Th 6514±448. n=3 animals each genotype.
Figure 4F	*TH+ GFP+/GFP+:* control 68±3%, *Pbx1*$^{Fl/Fl}$ 44±2%. n=5 control animals, 12 mutant animals.
Figure 4J	*Dendrite length (μm)*: *Pbx*$^{+/+}$: 684±97, *Pbx1*$^{Fl/Fl}$: 392±91. *Dendrite volumen (μm*^{2}*): Pbx*$^{+/+}$: 331±57, *Pbx1*$^{Fl/Fl}$: 81±21. *Total branching points*: *Pbx*$^{+/+}$: 44±7, *Pbx1*$^{Fl/Fl}$: 27±6. *Maximum cell-radius* (*μm): Pbx*$^{+/+}$: 64±5, *Pbx1*$^{Fl/Fl}$: 43±5). n=14 cells from three different control animals, and 12 cells from three different mutant animals.
Figure 5C	*GAD67+ GFP+/GFP+:* control 52±1%, *Pbx1*Th 73±1%. n=3 animals each genotype.
Figure 5F	*CR+ GFP+/GFP+:* control 4±0.3%, *Pbx1*Th 13±3%. n=3 animals each genotype.
Figure 5I	*CB+ GFP+/GFP+:* control 10±1%, *Pbx1*Th 10±1%. n=3 animals each genotype.
Figure 6A	*Time sniffing (s):* control 1.3±0.3 (oil) and 3.4±0.3 (geraniol), *Pbx1*Th 1.2±0.3 (oil) and 2.1±0.7 (geraniol). n=5 control animals and 8 mutant animals.
Figure 6B	*Time sniffing (s):* control 0.7±0.3 (oil) and 1.4±0.5 (carvone), *Pbx1*Th 0.8±0.3 (oil) and 0.9±0.6 (carvone). n=9 control animals and 8 mutant animals.
Figure 6C	*Time to descend (s):* control: 15.4±1.3, *Pbx1*Th 14.5±1.2. n=13 control animals and 10 mutant animals.
Figure 6D	*Total distance (cm*): control 380±23, *Pbx1*Th 315±21. *Entries in the center*: control 26±7, *Pbx1*Th 25±3. *Speed at the center (cm/s*): control 0.68±0.13, *Pbx1*Th 0.45±0.09. *Speed at periphery(cm/s*): control 0.28±0.02, *Pbx1*Th 0.25±0.02. *Time in the center:* control 2.8%, *Pbx1*Th3.9%. n=7 control animals and 6 mutant animals.
Figure 6E	*Buried marbles*: control 2±0.35, *Pbx1*Th 2±0.27. n=10 control animals and 6 mutant animals.
Figure 8G	*TH+ GFP+/GFP+:* Control + CRE 68±3%, *Pbx1*$^{Fl/Fl}$+CRE 44±2%, *Pbx1*$^{Fl/Fl}$+CRE+*Pbx1a* 68±2%, *Pbx1*$^{Fl/Fl}$+CRE+*Pbx1b* 47±9%. n= 5, 12, 4 and 4 animals respectively.
Figure S5	*Relative expression levels:* control 1±0.06, *Pbx1*Th 0.9±0.07. n=4 control animals and 3 mutant animals.